

University of Central Florida

STARS

Honors Undergraduate Theses

UCF Theses and Dissertations

2022

Novel Microbe-Resistant Clay Dressing for Healing Burn Wounds

Kasey L. Rigby

University of Central Florida



Part of the [Environmental Microbiology and Microbial Ecology Commons](#)

Find similar works at: <https://stars.library.ucf.edu/honorsthesis>

University of Central Florida Libraries <http://library.ucf.edu>

This Open Access is brought to you for free and open access by the UCF Theses and Dissertations at STARS. It has been accepted for inclusion in Honors Undergraduate Theses by an authorized administrator of STARS. For more information, please contact STARS@ucf.edu.

Recommended Citation

Rigby, Kasey L., "Novel Microbe-Resistant Clay Dressing for Healing Burn Wounds" (2022). *Honors Undergraduate Theses*. 1193.

<https://stars.library.ucf.edu/honorsthesis/1193>

NOVEL MICROBE-RESISTANT CLAY DRESSING FOR HEALING BURN
WOUNDS

by

KASEY RIGBY

A thesis submitted in partial fulfillment of the requirements
for the Honors in the Major Program in Biomedical Sciences
in the College of Medicine
and in the Burnett Honors College
at the University of Central Florida
Orlando, Florida

Spring Term, 2022

Thesis Chair: Kausik Mukhopadhyay, Ph. D.

ABSTRACT

Every year, about 550,000 patients receive medical attention for minor and major burns in the United States.¹ In 2020, it was estimated that 11 million people worldwide suffered from burn injuries, with 150,000 of those burns being fatal.² Burns are among the most painful and debilitating recalcitrant wounds that can often turn terminal when infection occurs. The different grades for burns that we aim to treat are first, second, and third degrees.² Each burn type is susceptible to secondary infection that can be life threatening, and as a result, are extensively treated with antimicrobial agents.² At present, only a handful of FDA-approved products are available in the market that can successfully treat second and third degree burn wounds and scars.³ Topical agents such as sodium hypochlorite, iodine, H₂O₂, silver etc. are used to combat burn wound infections.³ However, the relentless emergence of antibiotic resistant strains of pathogens, often with multiple antibiotic resistances together with the discovery of novel antibiotics, has necessitated investigating and developing better alternative treatments.

In this effort, a cost-effective approach to engineer a microbe-resistant bandage system utilizing clay was undertaken as the research project. This unique microbe-resistant material has been developed using organo-modification and metal-ion exchanged clay scaffolds, and has been fully characterized using analytical techniques such as powder XRD, ATR-FTIR, XPS, ICP-OES etc. The hybrid clay samples have also been tested for their antimicrobial efficacy against *Escherichia coli* (gram-negative) and *Staphylococcus aureus* (gram-positive) bacteria in promoting the process of wound healing to serve as a representative of the ESKAPE group of bacteria, which includes *Enterococcus faecium*, *Staphylococcus aureus*, *Klebsiella pneumoniae*, *Acinetobacter baumannii*, *Pseudomonas aeruginosa*, and *Enterobacter* species. By leveraging the

excellent hydrophilic and moisture retention properties of clay, we can postulate achieving optimal moisture transport from the dressing through the wound area to accelerate the healing cascade by hassle-free self-application at the point of injury.⁴

The proposed research deals with the antimicrobial effects conferred onto the clay matrix that can be used for the treatment of burn injuries and scars. Currently, most burn treatments involve high doses of silver-based products that make them costly.³ Moreover, most of these treatments are ointment-based, which exposes the wounds to cross-contamination when in contact with dust, debris, moisture, water, liquids, particulates etc. The goal is to develop a free-standing film composed of controlled amounts of silver ions tethered to the clay scaffolds that can be used to treat severe burns and scars. Performing animal studies using *in vivo* models for first or second degree burn injuries and scars exceeded the budget for this project, hence, antimicrobial efficacy against ESKAPE pathogens, *viz.* gram-negative and gram-positive bacteria using the engineered hybrid films was the focal point for this project. This unique and cost-effective system is much cheaper compared to ointments and other bandage systems. Moreover, the meso- and micro-porosities present within the clay can be easily leveraged for easy moisture and oxygen transport from bandage to skin, which is essential for natural healing of the wounds and burn injuries.⁴ Additionally, the antimicrobial/ antibacterial efficacy of this unique bandage system can be suitable for prolonged use, thereby minimizing the inconveniences of frequent changing and reapplication. This helps to reduce the risk of infection and contamination, drastically. Furthermore, the clay bandages will be mechanically more durable due to the nature of the highly structured layers in clay.

Clay has the well-known property of retaining moisture and has been used as a promoter for hemostasis, thereby, helping the composite films to serve multiple purposes in the burn and scar healing process.⁷ The hydroxyl groups in the clay used will be functionalized with trimethyl glycine (Betaine), expanding the clay galleries through intercalation, while Group II metal ions and silver ions can be easily exchanged with the sodium cations present in clay within the interstitial space. The metal ions (Ag⁺) exchanged organo-clay gallery is the main driving force for eliminating the microbes or bacteria. Thus, one of the prime goals for this effort is to develop an organo-modified Betaine-composite film that can be conformable to various shapes and sizes and will garner anti-microbial/ bacterial/ fungal properties. Other goals include developing films with optimal metal ion concentrations in the clay scaffolds to reduce the cost (by replacing Ag⁺ ions with group II metal ions in the silicate scaffolds) without compromising the efficacy of the product.

This research exhibits a novel, cost-effective solution to engineer microbe-resistant “hybrid” clay membranes by chemical modification, metal incorporation, intercalation, and exfoliation of clay-silicate galleries to prevent infections from ESKAPE pathogens. Results from the physico-chemical analyses have shown mechanical durability of the films. Antimicrobial efficacy tests using *Escherichia coli* (gram-negative) and *Staphylococcus aureus* (gram-positive) showed a significant reduction in bacterial growth, which indicates the antimicrobial efficacy of the clay films. In typical bacterial kill study experiments, the zone of inhibition was at or above 1 cm for both the gram-positive and gram-negative bacteria, with four samples tested with three 0.6 cm diameter discs against a clay control. Evidently, these matrices are effective at preventing the growth of bacteria that can prove to be infectious. This unique “hybrid” bandage system promotes:

(a) prevention and control of both gram-negative and gram-positive bacteria, (b) nontoxic and biodegradable features, (and c) easy application on wounds. X-Ray photoelectron spectroscopy is used to determine the quantitative elemental analysis, and binding energies and oxidation states of the elements. Powder X-Ray diffraction, ATR-FTIR, X-Ray fluorescence spectroscopy and viscosity have been used to determine physical properties, structures, and mechanical durability of the films.

ACKNOWLEDGEMENTS

I am thankful for the many people who aided in the formulation of this thesis. Many members of the Functional Hybrid Materials team led by Dr. Mukhopadhyay have helped me in several ways; Suvash (Ghimire) for helping me with the collection and interpretation of data presented in my thesis, Pritha (Sarkar) for proofreading and editing the drafts, and my ex- lab mate Jodie (Chen) for carrying out many experiments and presentations together. I would like to thank Dr. Elizabeth Brisbois and Manjyot Kaur Chug at University of Georgia (Athens, GA) for carrying out the antimicrobial tests in their lab in collaboration, which is an important segment of my thesis. Sincere thanks to my parents, Emily and Douglas Rigby, have provided immense support throughout this process.

I would also like to acknowledge the Burnett Honors College, College of Medicine, Department of Material Sciences and Engineering and Materials Characterization Facility at the University of Central Florida (UCF) for allowing me to carry out my research work in these labs. Special thanks to the Office of Undergraduate Research (Fall Undergraduate Research Grant), the College of Engineering and Computer Science (Honors Undergraduate Thesis Scholarship Award), UCF Student Scholar Symposium (Judges Choice Award) and American Chemical Society Orlando chapter (Best Undergraduate Student award) for their financial support pursuing my research and presenting in conferences.

My friends, including Peyton, Dan, Macey, Bob, and Dennis, assisted me in both proofreading and general support. They all made the late nights a little easier to power through.

Finally, I would like to thank my mentor and thesis Chair, Dr. Kausik Mukhopadhyay for his constant support and encouragement during the course of this work, and allowing me to think and pursue my work, independently. Special thanks to my Thesis Committee, Dr. Kaitlyn Crawford; without their advice this thesis would not have achieved the quality that it has.

I will be forever appreciative of the guidance from everyone that has helped me, both in and out of the lab; without the support of those listed above, and many others, I would have never been able to complete this thesis. I would not have traded this experience for anything in the world; I have learned so much throughout my time in the Mukhopadhyay lab, and I am grateful to have had the opportunity to contribute to the wider body of scientific knowledge regarding clay science with this thesis. I am looking forward to expanding my horizons even further at UCF College of Medicine upon graduation in Spring 2022.

TABLE OF CONTENTS

ABSTRACT.....	II
LIST OF FIGURES	VIII
LIST OF TABLES	IX
LIST OF ABBREVIATIONS.....	X
LIST OF EQUATIONS	XI
CHAPTER 1: INTRODUCTION.....	1
CHAPTER 2: LITERATURE REVIEW	4
CHAPTER 3: ANALYTICAL FUNDAMENTALS.....	19
CHAPTER 4: EXPERIMENTAL METHODS	30
CHAPTER 5: RESULTS.....	35
CHAPTER 6: DISCUSSION.....	46
CHAPTER 7: CONCLUSION	50
CHAPTER 8: MOVING FORWARD.....	52
REFERENCES	53

LIST OF FIGURES

Figure 1: A representation of skin anatomy. Adapted from National Institute of General Medical Sciences. ⁹	4
Figure 2: A representation of the inner structure of a mineral made of repeating tetrahedral and octahedral layers, such as kaolin clay. Adapted from Schoonheydt, et al. ¹⁵	8
Figure 3: A representation of the inner structure of a mineral made of repeating tetrahedral, octahedral, tetrahedral layers, such as montmorillonite clay and the exchangeable cations. TOT type clay is functionalized in this experiment. Adapted from Schoonheydt, et al. ¹⁵	9
Figure 4: Sample CAT-8 after peeling in bag (left) and on glass plate (right).....	35
Figure 5: Sample CAT-2 after peeling in bag (left) and on glass plate (right).....	35
Figure 6: Sample CAT-7 after peeling in bag (left) and on glass plate (right).....	36
Figure 7: XPS survey scan for Bentonite (control), Ag ⁺ (High conc.)-Clay-Betaine, Ag ⁺ (Low conc.)-Clay-Betaine, Clay-Betaine (High conc.), and Clay-Betaine (Low conc.).	38
Figure 8: XRD data for CAT-69 (Ag-1), CAT-69 (Ag-2), CAT-69 (Ag-3), CAT-69 (Ag-4), and the Bentonite Control.....	39
Figure 9: ATR-IR of sample CAT-69 (Ag-1), CAT-69 (Ag-4), and the bentonite control.....	42
Figure 10: Control Samples AB-1-13 Kirby-Bauer disc diffusion against <i>S. aureus</i> (Left) and <i>E. coli</i> (Right).....	43
Figure 11: From left to right, samples CAT-69 (Ag-1), CAT-69 (Ag-2), CAT-69 (Ag-3), and CAT-69 (Ag-4) Kirby-Bauer disc diffusion against <i>S. aureus</i>	44
Figure 12: From left to right, samples CAT-69 (Ag-1), CAT-69 (Ag-2), CAT-69 (Ag-3), and CAT-69 (Ag-4) Kirby-Bauer disc diffusion against <i>E. coli</i>	44

LIST OF TABLES

Table 1: Select clay film samples and their composition	31
Table 2: The compositions of the samples that were utilized in viscosity testing.....	33
Table 3: XPS binding energy values and their corresponding element and interpretation that are of interest to this experiment.....	37
Table 4: d_{001} -Values for the XRD data and the corresponding values that were used in calculations for the d_{001} -Values.	40
Table 5: Chemical composition of Ag-clay sample (in percentage).....	40
Table 6: ICP-OES data.....	41
Table 7: Viscosity data.....	43
Table 8: Data for the Kirby-Bauer disc diffusion against <i>S. aureus</i>	44
Table 9: Data for the Kirby-Bauer disc diffusion against <i>E. coli</i>	45
Table 10: ICP-OES Silver Data	47

LIST OF ABBREVIATIONS

TO	Tetrahedral-Octahedral
TOT	Tetrahedral-Octahedral-Tetrahedral
XPS	X-Ray Photoelectron Spectroscopy
XRD	X-Ray Diffraction
XRF	X-Ray Fluorescence
ICP-OES	Inductively Coupled Plasma Optical Emission Spectrometry
ATR-FTIR	Attenuated Total Reflectance coupled with Fourier Transform Infrared
ESKAPE	<i>Enterococcus faecium</i> , <i>Staphylococcus aureus</i> , <i>Klebsiella pneumoniae</i> , <i>Acinetobacter baumannii</i> , <i>Pseudomonas aeruginosa</i> , and <i>Enterobacter spp.</i>

LIST OF EQUATIONS

1. Bragg's equation
2. Rearrangement of Bragg's equation for the d value
3. X-Ray intensity calculation
4. Radiation absorption by an element calculation for XRF
5. Radiation intensity absorption calculation for XRF
6. Distance that radiation penetrates a sample calculation for ATR-FTIR
7. Penetration depth per reflection calculation for ATR-FTIR
8. Beer-Lambert Law

CHAPTER 1: INTRODUCTION

Burn wounds are among the most intensive injuries in regards to the cost, treatment, and additional medical issues post-injury, including infection and psychological effects.⁴ Those most prone to being burnt are women and children in middle- or low-income countries; resultingly, affordable treatment for burns is essential to prevent burn-related mortalities.¹ However, many of the treatments can be prohibitively expensive, especially when antibiotics are used.⁵ Many of these burn treatments include the use of silver-based ointments and creams, which deliver large amounts of silver to the wound site in order to combat infection. However, this large dosage can lead to issues such as antibacterial resistance.

As a result, the development of a cheaper and more accessible alternative to the current treatments is essential to the future care of burns across the world. Clay is a cheap, effective vehicle for many different types of medications.⁶ Consequently, silver cations already used to treat burn wounds may be an effective way to treat burn wounds. Being ubiquitous and inexpensive, a clay-based system would provide a much more cost-effective treatment for burn wounds. Clay also provides hemostatic effects by initiating the coagulation cascade.⁷ Overall, clay provides an incredibly effective method for treating serious wounds.

The goal of this research project is to develop a free-standing, hybrid clay-based film composed of controlled amounts of silver ions tethered to the silicate scaffolds in clay that can be used to treat severe burn wounds and scars. By treating the clay with trimethyl glycine (Betaine), the clay galleries get expanded through intercalation.⁸ By leveraging the exfoliation of clay and expansion of its galleries by intercalation of Betaine and various metal ions, esp. silver ions (Ag^+),

which can easily be exchanged with the sodium cations present in clay within the interstitial silicate lattice, Ag^+ cations can be incorporated into a synthesized hybrid clay film.⁷ The Ag^+ ions are well-known antimicrobe, which when incorporated in the clay galleries, will serve as the main driving force for eliminating the microbes or bacteria.

The synthesis of a hybrid clay film that includes Betaine and silver cations was confirmed by physico-chemical analyses, including X-Ray photoelectron spectroscopy, to determine the qualitative elemental analysis, and binding energies and oxidation states of the elements present therein. Powder X-Ray diffraction, ATR-FTIR, X-Ray fluorescence spectroscopy and viscosity have been used to determine physical properties, structures, and mechanical durability of the hybrid clay films. The successful synthesis of hybrid clay films with intercalated silver was confirmed prior to antimicrobial testing.

The antimicrobial tests aim to test a gram-positive and a gram-negative representative to demonstrate efficacy against the ESKAPE pathogen family, which is made up of *Enterococcus faecium*, *Staphylococcus aureus*, *Klebsiella pneumoniae*, *Acinetobacter baumannii*, *Pseudomonas aeruginosa*, and *Enterobacter* species. Antimicrobial efficacy tests using *Escherichia coli* (gram-negative) and *Staphylococcus aureus* (gram-positive) showed a significant reduction in bacterial growth, which indicates the antimicrobial efficacy of the clay films against both types of bacteria.

This research exhibits a novel, cost-effective solution to engineer microbe-resistant “hybrid” clay membrane by chemical modification, metal incorporation, intercalation, and exfoliation of clay-silicate galleries to prevent infections from ESKAPE pathogens. This unique

clay bandage system promotes: (a) prevention and control of both gram-negative and gram-positive bacteria, (b) nontoxic and biodegradable features, and, (c) easy application on wounds.

CHAPTER 2: LITERATURE REVIEW

2.1 BURN/BURN WOUNDS

In 2020, it was estimated that 11 million people worldwide suffer from burn injuries, with 150,000 of those burns being fatal, according to the World Health Organization.¹ Burns cause tissue damage by heat, chemicals, electricity, or radiation. Burn degree of the burn wound varies by the depth and size of the injury in relation to the layers of the skin (Figure 1).⁹ First-degree

burns are ones that only damage the outermost layer of the skin known as the epidermis, and they will heal within a week without any intervention.⁹ Second-degree burns are those that damage both the epidermis and a portion of the inner layer of the skin known as

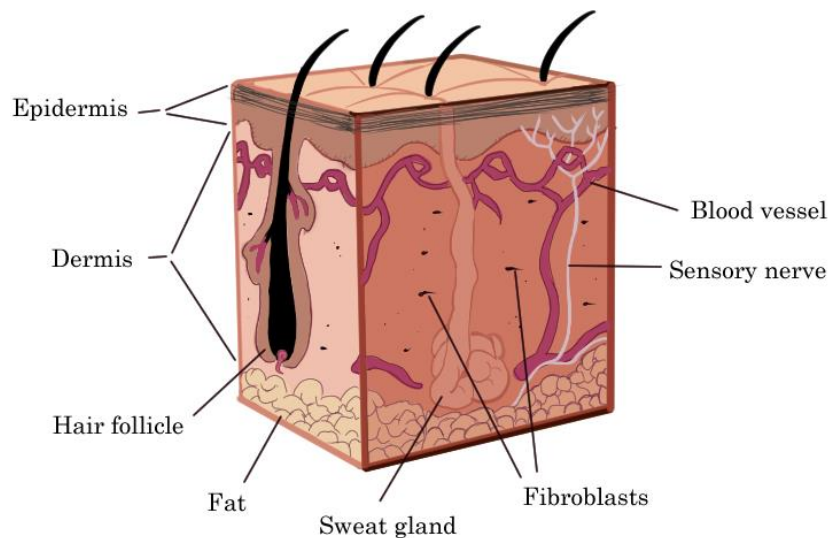


Figure 1: A representation of skin anatomy. Adapted from National Institute of General Medical Sciences.⁹

the dermis without damaging sweat glands or hair follicles.⁹ These types of burns may require a skin graft and bandaging to protect the damaged region of the skin. Third-degree burns damage the epidermis and dermis and extend to damaging sweat glands and hair follicles. Third-degree burns always require skin grafts and further treatment to ensure proper healing. Fourth-degree burns extend past skin into the fat layer, fifth degree burns damage muscle, and sixth-degree burns extend to the bone. Skin grafts are used to heal burns and help prevent scarring. Skin grafts are

patches of skin transferred from one area of the body to another to aid in healing.¹⁰ Burns can cause an extensive inflammatory response resulting in fluid loss and a severe drop in blood pressure leading to shock. Fluids can also be trapped within the body and cause edema, which can lead to organ failure.¹

Typically wounds progress through three stages of healing, the inflammatory/reactive stage, the proliferative/repairative stage, and the maturation/remodeling stage.¹¹ The inflammatory stage involves a response from the body, wherein more fluid containing red blood cells, leukocytes, and other proteins is brought to the injury site to initiate the healing process, including both blood and the lymph.¹¹ Following the inflammatory phase, the reparative phase involves the repair of epithelial tissue and covers the wound site. Finally, the remodeling phase involves scar formation by the accumulation of structural proteins.¹¹ Notably, burns increase capillary permeability, most likely caused by the damaging of capillaries due to excess heat, which can leak into the interstitial space and causing edema.¹¹ This significant fluid loss from edema can lead to shock, whereas in other wound types, shock is a result of overall blood loss from the wound opening. Most shock instances in burn victims result from this type of edema instead of classic hypovolemic shock.¹¹ This edema is also the basis for blister formation, wherein the epidermis remains intact. At the same time, the burn damages the dermis, and fluid accumulates from damaged capillaries beneath the epidermis layer.¹¹ There is also a less immediate complication with burns - the risk of infection that can be more dangerous and deadly than shock or edema. Burns directly damage skin, which is the body's first line of defense against pathogens. In addition, bacteria such as *Staphylococcus* and *Streptococcus* strains colonize the skin's surface, and when the skin breaks, infection is a high risk.⁹

Burns weaken the immune system due to an immune response that deviates from the norm.¹² The suppression of both the innate and adaptive immune systems significantly increases the susceptibility to infection.¹² Burn injuries damage the protective lining of the skin and epithelial cells, causing an increased vulnerability to infection due to the decreased innate defenses. Most cases of patients with severe burns involving 40% of total body surface area burns result in death caused by sepsis due to subsequent infection.¹³ The immune system's initial response to any wound is an inflammatory response. However, every degree of burn causes an inflammatory response that can be catastrophic, causing fluid loss through damaged capillaries, which induces shock or organ failure due to edema.¹³ Following this initial response, there is an anti-inflammatory effort to return the body to physiological homeostasis. As a result, both the innate and adaptive immune responses are repressed by the anti-inflammatory effort.¹³ This repression prevents a significant response to infection after the initial burn. This repression can also lead to infections at the burn site or in other tissues of the body, such as the lungs or bloodstream.¹³

In the initial response to a burn injury, the innate immune system activates, and phagocytes respond at the injury site.¹³ This innate response includes activity from dendritic cells, monocytes, and neutrophils that cause inflammatory response at the site of injury. In addition, the dendritic cells can activate the adaptive immune system by presenting antigens and recruiting T and B cells.¹³ Overall, both the innate and adaptive immune systems are highly active during the first response to a burn wound. However, if this immune response is prolonged, there can be significant damage done to already affected tissue and contribute to chronic diseases. Thus, the immune response must be repressed following the initial response. The immune response repression results in reduced chemotaxis of monocytes, low levels of dendritic cells, and reduced response by

macrophages.¹³ However, over-repressing the immune response too much or too soon can lead to significant infections, which is seen in the case of burn wounds and can be deadly.

The movement of monocytes is repressed in burn victims, which may be due to alterations in membrane protein expression in the monocytes as a result of the response to a burn injury.¹³ Due to the altered expression in monocytes, cytokine release is greatly decreased, which also depresses the movement of immune system cells and prevents a phagocytic response.¹³ The reduced movement of monocytes leads to a decreased number of monocytes at the site of injury. This reduction leads to a diminished immune response at the burn site and can lead to the potential uninhibited spread of infection throughout the body. Dendritic cells are hypothesized to be depleted through an apoptosis pathway or oxidative stress during a burn injury, and therefore much of the adaptive immune response is suppressed.¹³ Macrophages, an integral part of the innate immune system, also have affected activity associated with burn severity. As burn severity increases, macrophage activity decreases, which severely decreases the response to infection.¹³ Since the amount of monocytes present is greatly decreased, the macrophage and dendritic population cannot be subsequently increased through monocyte differentiation into macrophages or dendritic cells, therefore these depleted populations cannot be remedied through differentiation of monocytes. .

Overall, burn victims have a higher susceptibility to infection due to altered immune system responses. Prevention of infection is integral to healing. For example, Huan et al. discuss the significant dangers of the current SARS-CoV-2 pandemic in conjunction with burns.¹⁴ Patients are at a higher risk of infection, including SARS-CoV-2, when treatments for burn injuries are performed in an enclosed environment and close contact.¹⁴ Alterations to current isolation and

treatment protocols during the pandemic need to be updated for burn victims due to the high vulnerability towards infections. In general, burn wound victims must be closely monitored in order to prevent the onset and development of serious infections to avoid deaths associated with infections post-burn.

2.2 CLAY CHEMICAL AND PHYSICAL STRUCTURE

Clay minerals are mostly crystalline layered silicates that compose many soils. Clay minerals are generally made of alternating sheets consisting of silicates, metal cations such as aluminum-III, and hydroxyl groups. A clay film, developed by chemical modification or functionalization of clay,

is a stable and durable strip of clay composed of ordered clay.¹⁵ Clay is made of different layers of tetrahedral and octahedral sheets, which are stabilized by a central

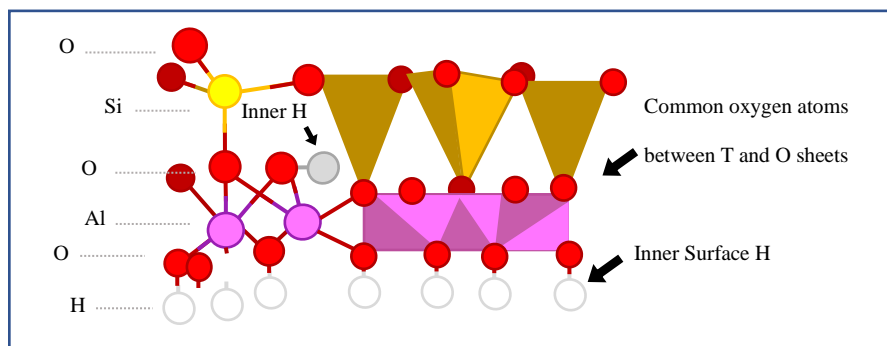


Figure 2: A representation of the inner structure of a mineral made of repeating tetrahedral and octahedral layers, such as kaolin clay. Adapted from Schoonheydt, et al.¹⁵

cation that is surrounded by anionic oxygen atoms.¹⁵ Some of the oxygen present in the clay layers can be protonated into a hydroxy group, depending on the pH of a solution.¹⁶ An acidic or alkaline spill on the clay can significantly impact the structural properties of the clay layers. For example, the functional group density of montmorillonite, one of the most common classes of clays, can be greatly increased when introduced to an alkaline environment and significantly change the pK_a of the clay.¹⁶ A result of this is the reduced ability of the clay layers to form a stable clay film. In

addition, the clay can lose octahedral cations in an acidic environment, which means cations intercalated within the clay layers can be lost in an acidic solution.¹⁶ Overall, a neutral environment is key to producing stable, workable clay films.

The sheets that make up a clay film can either be tetrahedral or octahedral. Tetrahedral sheets comprise a central silica atom that is surrounded by four oxygen atoms arranged in a tetrahedral geometry. Octahedral sheets are comprised of a metal cation center surrounded by four oxygens, some of which are in the octahedral conformation.¹⁵ Some of the oxygens in the octahedral group are in plane with the tetrahedral group, sharing an edge and forming the bond between the two layers. Clays can be found in a *tetrahedral-octahedral* (TO or 1:1) or a *tetrahedral-octahedral-tetrahedral* (TOT or 2:1) layering mineral.¹⁵ The

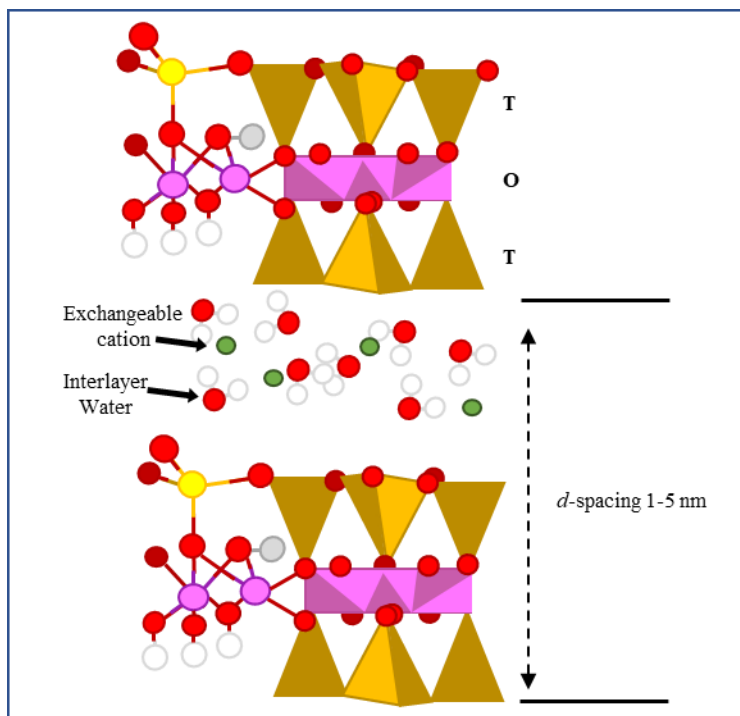


Figure 3: A representation of the inner structure of a mineral made of repeating tetrahedral, octahedral, tetrahedral layers, such as montmorillonite clay and the exchangeable cations. TOT type clay is functionalized in this experiment. Adapted from Schoonheydt, et al.¹⁵

molecular structure of TO and TOT layers can be seen in Figures 2 and 3. In the TO structure, the tetrahedral sheet is connected to an octahedral

sheet, and the pattern is repeated. A prominent example of a TO structured clay is kaolin, which is generally found in Georgia and South Carolina in the United States.¹⁵ TOT clay has an

octahedral sheet sandwiched between two tetrahedral sheets, and this pattern repeats.¹⁵ The stacking of the clay layers leads to open space between the layers, called the gallery or interlayer.¹⁷ Specifically, the presence of cations between the clay layers creates the spacing of the gallery, and a single interlayer space is called the basal spacing or d_{001} -spacing.¹⁸

There are various types of clay for either the 1:1 or the 2:1 structure with altered charges and attributes. The TOT clay used in this research was smectite clay, Montmorillonite and Bentonite being the most commonly known clays in the Smectite family.¹⁸ Smectite clay has a higher swelling capacity compared to other 2:1 and 1:1 clays, owing to the spontaneous increase of the d_{001} -spacing due to absorption of molecules in the interlayer space that allows intercalation of different materials and functionalization of the clay in the form of films.¹⁹ Smectite clays are uniquely hydrophilic due to a large number of silicates, which create more opportunities for hydrogen bonding with water, thus drawing more water in for more swelling.¹⁹

Overall, the clay layers are held together through van der Waals forces. Since these forces are relatively weak, the space between the layers that make up the clay structure can be subject to swelling through hydration.²⁰ Hydration causes water molecules to enter the space between the layers, which increases the basal spacing between layers, known as swelling.²⁰ The partial charges on water molecules can interact with the charged surfaces of the clay layers and cause the expansion of space between individual clay layers.²⁰ Simulated environments demonstrate that in Montmorillonite clay, the van der Waals interactions between clay layers decrease dramatically as water is added, illustrating the increased distance between layers and subsequent expansion of basal spacing between those layers.²⁰

Exfoliation is the process in which individual clay nanolayers are formed.²¹ Clay nanolayers have several advantages over aggregates of clay. Specifically, the barrier properties of clay are greatly enhanced when the clay is exfoliated.²¹ The simplest process of exfoliating clay includes the hydration of the clay aggregates followed by drying.²¹ Due to water having a protic nature with a partial negative charge localized on the oxygen, water molecules become bound to the metal ions present in clays, usually Na⁺ cations.²¹ Water enters the interlayer space where the cations reside, which causes an expansion of the clay layers followed by a delamination of the present cations. The addition of water serves not only to cause swelling in the clay layers, but also to encourage the exfoliation of the clay system.²¹

Using clay alone is not an efficient bandage system. Due to the structure of clay and clay layers, clay can be functionalized to cause the film to act as an antimicrobial system. Cation exchange is an aspect of clay that can be useful to functionalize clay films.²² Due to the negatively charged nature of clay caused by the anionic oxygen atoms, positively charged metallic ions are present in the gallery, such as sodium ions. The cations present between the clay layers can be exchanged with other types of cations with specific properties.²² Additionally, through swelling, larger metal ions and other molecular structures can be intercalated between the clay layers.²² By inserting these metal ions between the layers, known as intercalation, the antimicrobial properties of the silver can be conferred to the engineered clay films.

The cation exchange capacity (CEC) of clay is a measure of the ability of clay to exchange metal cations present within the clay layers with other types of cations.²² Due to the generally negative charge present on the surface of clay layers due to hydroxy functional groups, cations are attracted to the clay.²² By introducing a high concentration of positively charged ions, it is possible

to exchange the cations already present in the clay layers. Therefore, it is possible to functionalize clay with more complex cations.

2.3 ORGANO-FUNCTIONALIZATION OF CLAY

Despite the ability to exchange cations within the clay gallery, the larger ions may have difficulty fitting within the interlayer spacing. A solution to this issue is the organo-functionalization of clay. The organo-functionalization of clay can be achieved by exchanging cations in the interlayer space with positively charged quaternary ammonium molecules²³. This ion exchange is fundamentally the same process as the functionalization of clay with single cationic atoms, with the positively charged ammonium groups adhering to the negatively charged surface of the clay layers.²³ The major difference between organo-functionalization and functionalization using metal ions is that the organo-functionalization process makes the clay more miscible with polymer matrices and significantly increases the basal spacing of the clay gallery.²³

The innate thickness of the organic cations will determine the interlayer spacing, with the larger quaternary alkylammonium ions corresponding with larger spacings.⁸ In addition, by utilizing a zwitterion with a positively charged end and a negatively charged end, the interlayer basal spacing can be increased even more due to the negatively charged groups repelling each other in the gallery and the positively charged groups adhering to the clay layer surfaces.⁸ The negatively charged groups can also interact with positive metal cations, encouraging the functionalization of the clays through the intercalation of the metal cations. Alternatively, long, uncharged alkyl chains impede clay swelling.⁸

Trimethyl glycine or carboxy Betaine (hereafter referred to as ‘Betaine’) is a quaternary ammonium zwitterion made of a modified version of the amino acid glycine.²⁴ By utilizing the unique properties of Betaine, it is possible to expand the layers between the lattices within the clay structure.⁸ Betaine’s zwitterionic structure allows it to bind to the clay platelets and act as a scaffold to increase the spacing between clay interlayers, thus allowing for larger molecules or structures to fit within the clay layers.⁸ Through the utilization of the positive and negative charges on Betaine (being a zwitterion), functionalization of the clay using silver and other metal ions is possible.²⁴ Betaine lacks a long alkyl chain and contains a negatively charged carboxyl group, increasing the interlayer basal spacing without disrupting the swelling capacity of a clay mineral.

2.4 CLAY WITH ANTIBACTERIAL PROPERTIES

Clays and clay slurries are known to be used in wound healing applications.⁴ Through both physical and chemical processes, clays can help defend open wounds from pathogens. Clay is nontoxic, adsorptive, swelling, chemically stable, and modifiable, and cation exchangeable.⁴ Specifically, smectites separate easily into discrete nanolayers, which can be used to create helpful clay films that contain cations that can be utilized for antimicrobial purposes.⁴

It has been shown that clay paste can help in the wound healing process, as reported by Dário et al.⁴ In addition, clay also has antibacterial properties that exhibit zones of inhibitions, specifically when hydrated. Clay can slowly release antibacterial materials from their porous layers over time; specifically, some clays containing particular metal cations show significant antibacterial properties.⁴

Physically, clay is a barrier between the wound and the surrounding environment by adhering tightly to the skin.²⁵ In addition, the negative surface charge of clay minerals can also deter the activity of pathogens through the exchange of positively charged ions.⁴ These positively charged ions are the key to clays' chemical process that allows them to act as antibacterial agents. It has been noted that the antibacterial character of clays is increased when hydrated, demonstrating the importance of the metal ions that are released when the clay mineral is hydrated.²⁶ Overall, clay minerals can act as an efficient vehicle in transporting the antibacterial metallic ions to the injury site.

2.5 ANTIMICROBIAL CLAY SYSTEMS PREVIOUSLY DEVELOPED

The properties of clay that lend it to performing as an effective vehicle for treatment(s) has already been explored in various ways. The use of clays as a foundation for composites in antibacterial treatment has been a recent subject of scientific study.²⁷ Chitosan [poly-(b-1/4)-2-amino-2-deoxy-*D*-glucopyranose], a biomolecule found in the shells of crustaceans, has been shown to have antimicrobial properties against a plethora of microbes.²⁸ Through the use of a quaternary ammonium intercalant agent, a chitosan/organoclay composite using montmorillonite was successfully synthesized, and said composite performed better in antibacterial tests than lone chitosan.⁶ Other materials such as polyurethane and various alkylammonium salts have also been shown to have bactericidal effects when incorporated into clay mineral systems.²⁹

The use of clay as a drug delivery system also provides certain advantages. For example, a drug-montmorillonite system favors release of the drug over time as opposed to an initial flood of a drug that could contribute to cytotoxic effects or rapid degradation in the body.³⁰ Therefore, in

combination with the swelling and cation exchange properties of bentonite clay, the combination of organo-functionalized clay with another antibacterial system can lead to greater antibacterial effects over a sustained period of time.

2.6 ANTIBACTERIAL SILVER

Silver topical agents are widely used to treat burns injuries. Silver has been shown to have a wide array of bactericidal and bacteriostatic effects against both gram-positive bacteria, gram-negative bacteria, and even biofilms.³¹ Silver has been known to have antimicrobial effects, and was commonly used for medical treatment since ancient times. It was used as early as 750 A.D. to treat cholera, and silver was first used in 1965 to treat burn wounds.³¹ It is believed that silver invades the cell's membranes, both inner and outer, then interferes with gram-positive bacteria cell walls, causing cytoplasmic leakage or interfering with microbial metabolism proteins of gram-negative bacteria, causing cell death.²⁴ Notably, it has been shown that silver affects the proton motive force and the electron transport chain of bacteria.²⁴ In addition, the anti-viral properties of silver are believed to be due to silver interfering with nucleic acid or viral proteins.²⁴

Metal complexes have been utilized to help treat different diseases throughout history.³² For example, arsenic was used to treat syphilis, as well as gold to treat arthritis.³² Silver is commonly used to prevent burn infections, but further research into different metals and the antimicrobial effects they may have is important to help develop new treatments and fight against antimicrobial resistances.³² Copper has shown great efficacy as a cancer treatment, and metal ions including cobalt, nickel, lead, and copper have been shown to have significant antimicrobial effects.^{32,33} Silver combined with different materials has been shown to increase the ability of silver

to act as an antimicrobial agent. Silver nanoparticles have been researched in recent years to determine the antimicrobial ability of silver when combined with other materials.³¹ When looking at clays combined with silver, zeolite, an aluminosilicate clay, has been demonstrated to have significant antimicrobial effects while also avoiding some of the pitfalls commonly associated with silver agents.³⁴ Silver-zeolite clay complexes are already commonly used in dental procedures.³⁴ Consequently, the combination of antimicrobial silver and clay provides a unique approach that could outperform the current methods of treatment.

2.7 SYNTHESIS OF CLAY FILMS

There are many ways to make clay films, including casting, spin coating, Layer-by-Layer (LbL) deposition, L.B. and L.S. methods, and more.³⁵ The casting method is the most straightforward method of synthesizing clay films. The clay is mixed within a solvent to make a clay solution, and the solution is spread out onto a surface with a flat bottom.³⁵ The solvent is then allowed to evaporate slowly, which leaves behind the clay layers. This is a simple way of making clay films; however, if the clay concentration is too high, aggregates of the clay will settle on the top of the film and make an opaque layer.³⁵ Due to the layered anionic hydroxides in the clay layers, cations can be incorporated in between the clay layers. When different types of cations were incorporated, different characteristics were observed in the films. Smooth and flat films were observed with montmorillonite with monovalent or divalent cations, such as Li^+ or Mg^{2+} .³⁵ When using montmorillonite with the trivalent Al^{3+} cation, the clay films were observed to be curved and shrunken.³⁵ The films came out as curled pieces when using iron, either with divalent or a trivalent cation.³⁵

Another way to create clay films is through spin coating.³⁵ This method of film creation uses centrifugal force to create even clay films.³⁵ The clay is suspended in an aqueous solution, which is then dropped onto the center of a disk that is spun at a high speed.³⁵ This method can be used to create very thin films, where the film thickness directly depends on the concentration of the clay.

The next method for creating clay films is the layer-by-layer deposition, also known as LbL deposition.³⁵ This method uses a surface that has a negative charge, such as with glass.³⁵ The surface is then submerged in a cationic polymer, which coats the surface with a positive charge. The now-positive surface is then submerged into a clay solution, where the clay is attracted to the positively charged coating due to the hydroxy groups in the clay, and a single clay layer is created.³⁵ This cycle is repeated until enough clay layers are layered to create a film.³⁵ The number of cycles as well as the concentration of the clay solution influences the thickness of the film.

The L.B. and L.S. methods take advantage of the Langmuir film.³⁵ This type of film is formed by suspending water-insoluble, amphipathic molecules in an organic solvent, which is then spread on an air-water interface. The air-water interface is the aqueous solution with clay.³⁵ The solvent evaporates, leaving the amphipathic molecules behind, which attract the clay through hydrophobic and electrostatic interactions. This process creates the clay film, which then can be extracted from the solvent by vertical dipping (L.B. method) or horizontal dipping (L.S. method).³⁵ Cations can then be incorporated into the clay film using a third cation component that exchanges the sodium ions in the clay with the chosen cation. The thickness and density of the cations in the clay film is controlled by the concentration of the aqueous clay solution.³⁵

Electrophoretic deposition is a method of using electrophoresis to create clay films due to the anionic nature of the clay layers. In addition, complex metal cations can be incorporated with the clay films.³⁵ Chemical deposition is a method of immobilizing clay layers on surfaces using silane coupling agents, which bind the clay layers using covalent bonds. Finally, suction filtration uses a suction funnel with a membrane filter, through which the clay solution is filtered. The clay is stuck to the membrane and can be peeled off the filter as a film.³⁵

The previously discussed concepts and processes can be combined to develop an effective clay film functionalized with organic molecules and antimicrobial metals. The challenge, however, is to create clay films that are both physically and chemically stable. Due to the simple procedures and little equipment required, this thesis work utilizes the casting method of creating a clay film.

CHAPTER 3: ANALYTICAL FUNDAMENTALS

In this thesis, a multitude of analytical methods were used to determine the composition, stability, and efficacy of synthesized clay films. The following analytical approaches were used to analyze the composition and structure of the clay film: X-Ray photoelectron spectroscopy, powder X-Ray diffraction, X-Ray fluorescence, inductively coupled plasma optical emission spectrometry, attenuated total reflectance coupled with Fourier transform infrared spectroscopy, and dynamic mechanical analysis. For the antimicrobial efficacy analysis of the hybrid clay films, Kirby-Bauer disc diffusion was used to study the inhibition zones resulting from the interaction of the clay films with gram-negative and gram-positive bacteria.

3.1 X-RAY PHOTOELECTRON SPECTROSCOPY (XPS)

X-Ray photoelectron spectroscopy, or XPS, is a method of analyzing a material's surface to determine the general elemental makeup and binding energy values of the elements present in the material. In a typical experiment, XPS is performed by bombarding the surface of a sample with photons, which causes electrons to be emitted from the elements of the sample.³⁶ The energy of the photons is absorbed by the solid, and if the energy required for an electron to escape is met or exceeded, then the electron is released from the surface.³⁶ This release of electrons when a material is hit by electromagnetic radiation is known as the photoelectric effect, and it serves as the basis of XPS analysis.³⁶ The kinetic energy of the released electron can be measured and used to calculate the binding energy of an electron. Since the binding energy of an electron changes depending on the element it is attached to, as well as the surrounding environment, the measured binding energy can be used to identify specific materials on the surface of a solid.³⁶ An XPS graph

is plotted in reference to the kinetic energy and the intensity of a signal. The XPS graph can then be utilized to define elements present.

This graph can indicate how much of the element that ejected the electron is present on the surface of a material, which can be used to confirm the presence or absence of a sufficient amount of an element. For this experiment, silver was utilized and should show up on an XPS analysis of the material. Notably, pure silver has a binding energy of 368.2 eV or 373.8 eV.³⁷ If this binding energy is detected in the sample, then silver is most likely present. Pure silver has two possible binding energies due to the different possible spin states of the silver in the *d* orbital shell. In addition, the presence of quaternary ammonium nitrogen with a binding energy of 401.6 eV indicates the successful incorporation of Betaine into the clay sample, as quaternary ammonium nitrogen is not naturally present within clay samples.³⁷

XPS analyzation directly depends on the distance an electron must travel through a sample. As a result, much of the XPS data retrieved will only report the elemental makeup of the surface of the material or directly below the surface.³⁶ To counter this, other analyzation methods can be used to determine the elemental composition of the whole sample.

3.2 X-RAY DIFFRACTION (XRD)

In addition to XPS, powder X-Ray diffraction (XRD) was also utilized to determine the structure and composition of the clay matrices. XRD bombards the material with X-Rays similarly to XPS; however, instead of measuring the bonding energy of a released electron, XRD analyzes the change in the amplification of the X-Ray that is diffracted by the material.³⁸ XRD reports data about the crystal structure of a material by extracting information from wave interference signals

that arise due to the arrangement of atoms within a structure.³⁸ Different arrangements of atoms will result in different intensities of corresponding X-Rays, which can be measured and utilized to determine the three-dimensional structure of a material.

The electrons of the atoms that makeup a powder will interact with the electric field of an X-Ray, and a resulting wave will be produced from the atoms. The resulting wave has an amplitude that is proportional to the electrons in the atom, which can be utilized to determine the atomic number, and thus the specific atom that is being struck by X-Rays.³⁸ Multiple X-Rays will be reflected and diffracted by multiple atoms, and the interaction of the different atoms within a material can alter the expression of the resulting wave. If the diffracted X-Rays are in phase, constructive interference will occur, and the amplitude will increase. If the diffracted X-Rays are out of phase, then destructive interference occurs, where the amplitude decreases to zero. In both destructive and constructive interference, the wavelength remains the same, and thus can be used to calculate the angle of diffraction. The constructive interference is utilized to measure the angle of diffraction through Bragg's equation.³⁸

$$n\lambda = 2d \sin \theta \quad [1]$$

Where λ is the wavelength, n is an integer that represents the diffraction order, d is the distance between lattice planes, and θ (theta) is the angle difference between the original X-Ray beam and the diffracted X-Ray beam.³⁸ As a result, the angle theta is determined by the distances between atoms in lattice planes. The intensity and the two-theta can be represented graphically and matched to specific materials such as quartz, different types of clay, and silver. Because Bragg's

equation is in relation to constructive interference, it can be used to index any peak of significant intensity within the XRD graph.³⁸

Rearranging equation [1] to find the d_{001} value gives equation [2]:

$$\frac{n\lambda}{2 \sin \theta} = d_{001} \quad [2]$$

Equation [2] will be utilized in the XRD analysis to determine the d -spacing of the synthesized clay films.³⁸

As mentioned previously, the d_{001} value (hereafter referred to as d_{001} -spacing) gives the distance between lattice planes. By measuring the d_{001} -spacing in the XRD of a control clay and comparing it to the d_{001} -spacing in the XRD of a Betaine-incorporated clay, it is possible to quantitatively determine the increase in basal spacing due to the introduction of Betaine.

3.3 X-RAY FLUORESCENCE (XRF)

X-Ray fluorescence (XRF) is a method of analyzing a material by bombarding the material with X-Rays, similar to XPS. However, in XRF, X-Rays are emitted by the material of interest, whereas in XPS, photons are emitted and measured. Individual elements have characteristic radiation from the incident X-Rays.³⁹

XRF is generally measured using the primary fluorescence of a sample, which is the beam of X-Ray photons directly expressed by the elements in the sample without any interaction with other elements in the sample.⁴⁰ The radiation exhibited by the sample will be characteristic for the element that produces the primary fluorescence.⁴⁰

In order to calculate the primary fluorescence of a sample, several parameters must be defined. First, the intensity of the X-Rays that reach the sample (I) can be defined as:

$$I = I_0 \exp(-\mu_s \rho x) \quad [3]$$

Where I_0 is the initial intensity, μ_s is the mass absorption coefficient of the whole sample when the same has reached the excitation energy, ρ is the sample density, and x is the pathlength of radiation.⁴⁰ Only a fraction of the radiation intensity that reaches a sample is absorbed by a specific element. The absorption by an element can be defined as:

$$\left[C_i \left(\frac{\mu_i}{\mu_s} \right) \right] (\mu_s \rho dx) = C_i \mu_i \rho dx \quad [4]$$

Because only a fraction of the sample is a specific element, μ_i is used to designate the mass absorption coefficient of a specific element, and the expression $\frac{\mu_i}{\mu_s}$ is used to find the fraction of the element that composes the whole sample.⁴⁰ This expression is then multiplied by the mass absorption coefficient of the specific element (C_i) to determine the absorption of a single element within the sample as a whole. The expression $\mu_s \rho dx$ expresses the radiation intensity absorbed by the sample, as not all of the intensity that reaches the sample is absorbed. Finally, $C_i \mu_i \rho dx$ expresses the simplification of this equation.⁴⁰

To determine the intensity of radiation that an element absorbs, equation [2] and equation [3] can be combined:

$$dI = I_0 (C_i \mu_i \rho dx) \exp(-\mu_s \rho x) \quad [5]$$

By multiplying I_0 by the absorption of a specified element in the sample, the total possible absorbance by that element is calculated and then the other parameters of the sample can be taken into account, and thus the intensity available to an element in a sample to produce primary fluorescence is calculated.⁴⁰

For primary fluorescence to be emitted by a sample, a K-shell electron must be ejected as well as emit $K\alpha$ radiation instead of $K\beta$, as $K\alpha$ is produced more frequently and will generally be measured in XRF.⁴⁰

The fluorescence given off by an element can be utilized to determine the elemental composition of a sample. However, XRF is only semi-quantitative, and can only detect surface-level composition. As a result, it is not ideal for determining the composition deeper within the sample. By using “thin-film” XRF, a method of XRF where a sample is ground into a powder and spread over a membrane, some of these problems can be minimized.⁴¹ Thin-film XRF can provide a solution to some issues, but it contains its own problems. There can be elemental interactions that cause different absorptions to be measured, as well as the particle size distribution being unequal.⁴¹ Without uniform particle size throughout the film, it can be nearly impossible to receive consistent readings between comparable samples due to different particle size distribution between the samples.⁴¹ Accordingly, a more accurate and precise method of analyzing the samples was adopted following preliminary XRF analysis.

3.4 INDUCTIVELY COUPLED PLASMA OPTICAL EMISSION SPECTROMETRY (ICP-OES)

Inductively coupled plasma optical emission spectrometry (ICP-OES) is a quantitative analysis of a whole sample due to the digestion of a solid with acid and conversion to an aerosol vapor. The vaporized sample can be quantitatively analyzed, and the whole composition can be calculated.

To perform ICP-OES, the solid sample must first be digested and acidified into a solution that is then aerosolized to travel through plasma.⁴² The plasma is generated by using elemental argon and using electric power to energize the gas into a plasma.⁴² The plasma heats the aerosol, causing the solvent to evaporate, and the particle being analyzed is left behind. An auxiliary gas is used to prevent the plasma from energizing and damaging the tube. The plasma heats the particle, and the particle is vaporized. The elements composing the analyte can be excited, which causes an electron to enter a higher orbital state. Once the electron returns to the ground state, photons are emitted and can be detected.⁴² Only a very small amount of particle is excited and can be detected through optical emission. The excitation of the electrons and subsequent electron relaxation emits a photon of specific energy associated with the element and elemental state of an atom.⁴² The resulting spectra is dispersed, and the intensities of the light can be analyzed against the background to quantitatively determine the composition of a sample.⁴²

Plasma is an ionized gas with free electrons, and the basics of gas laws should apply. The temperature of the gas indicates the kinetic energy, which controls the transfer of energy to the sample therefore controlling the optical emission of the sample.⁴² The temperature of the plasma is dependent on the pressure, the electron concentration, and the gas temperature, assuming that the electron temperature is the same as the gas temperature.⁴² Knowing the energy of the plasma

as it relates to the energy being absorbed by the sample is essential for getting a proper measurement of the optical emission of the sample.⁴²

The liquid sample is converted into an aerosol by passing through a nebulizer prior to being introduced to the plasma. The plasma must be able to vaporize the solution, which can only occur if the volume of droplets is very small. Much of the errors that are measured in ICP-OES are a result of incorrect aerosol generation. In most ICP-OES machines, the aerosol is generated in a nebulizer that only allows small drops of aerosol to be introduced to the plasma and be vaporized. The speed at which the sample is introduced to the nebulizer as well as the gas flow rate in the nebulizer affect the efficiency of the ICP-OES process. Generally, a slower sample uptake and a faster gas flow rate results in smaller aerosol droplets and a more efficient aerosol transport.⁴² Finally, the background must be measured to ensure possible corrections for trace element amounts.

ICP-OES gives a more detailed profile of the elemental components of a sample than XRF the initial XRF measurements were followed by ICP-OES. Both of these processes utilize the optical emission of a sample, but ICP-OES is quantitative whereas XRF is qualitative. ICP-OES is thus more reliable in measuring the contents of a sample.

3.5 ATTENUATED TOTAL REFLECTANCE COUPLED WITH FOURIER TRANSFORM INFRARED (ATR-FTIR)

Attenuated total reflectance (ATR) coupled with Fourier transform infrared (FTIR) spectroscopy was used to further analyze the structure and organo-functionalities of the hybrid clay films. (FTIR) spectroscopy characterizes the surface of a material. In FTIR, infrared light is

transmitted in a beam onto a sample, where the bonds present will stretch, bend, twist, and be absorbed.⁴³ Depending on the bonds present in a sample, different amounts of infrared light will be absorbed. ATR is a method of analyzing a material through the refractive index of a sample. To accomplish ATR, a sample is placed on an internal reflection element (IRE) with a known, high refractive index. Infrared light is reflected through the IRE and onto the material, which will reflect the light back onto the IRE with a specific angle.⁴⁴ By utilizing an angle greater than the critical angle, the infrared light in the sample will undergo internal reflection. The result of that internal reflect is an evanescent wave that is absorbed by the sample and becomes attenuated.⁴⁵ The distance that the radiation penetrates a sample can be calculated using a formula:

$$b' = Nd_p \quad [6]$$

Where b' is the calculated path length, N is the number of reflections, and d_p is the penetration depth per reflection.⁴⁵ Furthermore, the d_p can be calculated thus:

$$d_p = \frac{\lambda_1}{2\pi n_1 [\sin^2 \theta - n_{21}^2]^{\frac{1}{2}}} \quad [7]$$

Where n_1 is the index of refraction of the IRE, n_2 is the index of refraction of the sample medium, n_{21} is n_2 divided by n_1 and λ_1 is λ_{vacuum} divided by n_1 .⁴⁵ Finally, the concentration of a sample can be taken into consideration when measuring the absorbance of the sample with a modified Beer-Lambert Law:

$$A = \epsilon cb' \quad [8]$$

Where A is the absorbance, ϵ is the molar absorptivity, and b' is the path length, as defined previously. Through measuring the absorbance of the sample as a whole and using the previously

stated equations, it is possible to determine the path length, which is then utilized to calculate the absorbance of specific bonds in the sample, as the path length is proportional to the absorbance of a sample.⁴⁵

The bonding information of the atoms can be used to confirm the successful incorporation and intercalation of Betaine into the clay layers through the presence of carbon-nitrogen (C-N) bonds that would not be present if the Betaine had not been incorporated.

3.6 VISCOSITY

The viscosity of a clay solution plays an important role in signaling that a clay film is likely to form. Viscosity of colloid suspension increases with edge-to-face or edge-to-edge interactions of clay layers. The neutral water solvent causes the edge-to-face associations to be more likely to occur, where the central metal of the face interacts with the edge hydroxy groups.⁴⁶ As previously stated, overly alkaline solvents can cause these interactions to be unable to occur due to the deprotonation of the hydroxy group on the edges of the clay layers. As these interactions increase, the likelihood of a formation of a clay film increases. This is because the edge-to-face or edge-to-edge interactions between the clay layers creates a “house-of-cards” structure that will cause the layers to associate more strongly and create a film.⁴⁶ Overall, these interactions promote the formation of a clay solution that is more viscous, and a thicker film that is more likely to adhere to itself is formed.⁴⁷

It can be hypothesized that the introduction of a zwitterion to the clay colloid suspension will decrease the overall viscosity of the solution by disrupting the “house-of-cards” flocs by interacting with the charged edges and faces of the clay layers. This creates a decrease in clay

interactions in solution while preserving the final film formation.⁴⁷ Therefore, a decreased viscosity in solution is expected, with a clay film with increased basal spacing being the expected result.

3.7 KIRBY-BAUER ASSAY

For this project, a Kirby Bauer assay was utilized to determine the antimicrobial efficacy of the functionalized clay films against both gram-positive and gram-negative bacteria groups. Gram-positive and gram-negative bacteria are defined by the color they turn when stained with crystal violet dye.¹² In a typical test, a peptidoglycan cell wall retains the purple or blue color, making them gram-positive.¹² Cells that lack a cell wall will not retain much color and instead will appear as pink and be classified as gram-negative. The treatment of gram-positive and gram-negative bacteria may differ, as certain antibiotics can only treat one type. For example, if the cell wall of a gram-positive bacteria is degraded, lysis of the cell most likely follows; however, there is not a significant cell wall to degrade in gram-negative bacteria, and they cannot be treated in the same way.⁴⁸ The Kirby-Bauer disk diffusion susceptibility test is a commonly utilized test to identify the bactericidal or bacteriostatic properties of materials. The test is carried out by inoculating a pathogenic organism on Mueller-Hinton agar as a spread, or ‘lawn’ plate, which contains a paper disk that contains the antimicrobial. The growth, or lack thereof, of the pathogenic organism around the paper disk indicates the efficacy of the antimicrobial. The area around the disk that lacks organism growth due to the antimicrobial is called the zone of inhibition, and the diameter of the zone of inhibition indicates the effectiveness of the antimicrobial.⁴⁹

CHAPTER 4: EXPERIMENTAL METHODS

4.1 SYNTHESIS OF ORGANO-FUNCTIONALIZED CLAY FILMS

In the experiment, clay films were developed through the casting method, where the clay is mixed in solution and then poured onto a glass surface, and the solvent is slowly allowed to evaporate. Different clay slurries were developed, with the control clay film with no metal cation exchange being developed first and serving as the basis for the development of the clay films with incorporated metals. To create the clay films, clay, water, and the metal ion that will be intercalated into the clay layers in the form of a metal salt are first combined as a solution, with the metal concentration being varied to measure the antibacterial efficacy of the film at different metal concentrations. silver nitrate was added to the clay to incorporate silver (Ag^+) ions.

In addition, variable amounts of Betaine were added to the slurry to determine the most effective and optimum concentration of Betaine exchanged clay. The clay slurry was allowed to mix at least 24 hours, which was followed by centrifugation using an OHAUS FC5718 with 6x50 mL rotors and decanting to remove the exchangeable cations (Na^+), as well as the released nitrate from the metal salt (AgNO_3). The centrifugation and decanting process was repeated until the liquid decanted was clear. After the centrifugation process, water is added to the remaining pellet, and then the slurry is again allowed to stir to ensure an even concentration throughout the slurry. The slurry is then cast and allowed to dry. Then, the film is carefully peeled, bagged, and labelled. Characteristic samples and their composition are listed in Table 1.

Table 1: Select clay film samples and their composition

Sample	Clay (mole)	AgNO₃ (mole)	Betaine (mole)
CAT-2	7.81×10^{-3}	0	4.93×10^{-3}
CAT-7	7.81×10^{-3}	0	2.47×10^{-3}
CAT-8	7.81×10^{-3}	0	7.40×10^{-3}
CAT-17	7.81×10^{-3}	0	4.10×10^{-3}
CAT-18	7.81×10^{-3}	0	5.92×10^{-3}
CAT-69 Ag-1	7.81×10^{-3}	8.83×10^{-4}	2.47×10^{-3}
CAT-69 Ag-2	7.81×10^{-3}	2.65×10^{-3}	2.47×10^{-3}
CAT-69 Ag-3	7.81×10^{-3}	5.30×10^{-3}	2.47×10^{-3}
CAT-69 Ag-4	7.81×10^{-3}	1.06×10^{-2}	2.47×10^{-3}
BAT-24 (very low Ag content)	7.81×10^{-3}	1.77×10^{-3}	4.93×10^{-3}
BAT-25 (low Ag content)	7.81×10^{-3}	5.30×10^{-3}	4.93×10^{-3}
BAT-26 (medium Ag content)	7.81×10^{-3}	1.06×10^{-2}	4.93×10^{-3}
BAT-27 (high Ag content)	7.81×10^{-3}	2.14×10^{-2}	4.93×10^{-3}

4.2 X-RAY PHOTOELECTRON SPECTROSCOPY (XPS)

The XPS procedure was performed using an ESCALAB-250Xi spectrometer equipped with Al-K α monochromatic X-Ray source (20 mA, 15 kV) and was operated at 300W in an ultra-high vacuum pressure chamber (7×10^{-9} mbar) at room temperature, while maintaining the spot size of beam at 650 μ m. The binding energy calibrations were done with reference to the C 1s peak at 284.6 eV. The Thermo Avantage Peakfit[®] software was used for the deconvolution of the spectra present in the samples. The spectra were fitted with a Gaussian-Lorentzian peak after the subtraction of a smart background. High resolution spectra were obtained using either a 10- or 20-deconvolution program, which varied the peak heights within an envelope over a complete range to determine the best fit, checked using the X² value to the actual data. Charge neutralization was deemed to have been fully achieved by monitoring the C 1s signal for adventitious carbon. A sharp main peak with no lower B.E. structure is generally expected. Instrument base pressure was $7 \times$

10^{-9} mbar. High-resolution spectra were obtained using an analysis area of $\approx 300 \times 700 \mu\text{m}$ and 20-eV pass energy. This pass energy corresponds to Ag $3d_{5/2}$ full width at half maximum (FWHM) of 0.55 eV.

The XPS was performed on the BAT-24, CAT-17, and CAT-18 to compare the effects of Betaine modulation as well as silver nitrate modulation.

4.3 X-RAY DIFFRACTION (XRD)

The instrument utilized for the powder XRD analysis was a Panalytical Empyrean X-Ray diffractometer with a copper X-Ray tube (Cu Ka of wavelength 0.1544426nm), and the data was collected between 5° to 50° at 5° per minute and a step size of 0.05. The data retrieval was done using an X'Celerator Multi-element detector. The samples utilized for XRD analysis were the CAT-69 group as well as a bentonite control.

4.3 X-RAY FLUORESCENCE (XRF)

The XRF analysis was performed on the CAT-69 sample group using a Panalytical Epsilon 1 with silver excitation source. To perform the XRF, the clay samples were placed in measure cups with $3.6 \mu\text{m}$ Mylar films.

4.4 INDUCTIVELY COUPLED PLASMA OPTICAL EMISSION SPECTROMETRY (ICP-OES)

To perform the ICP-OES, the CAT-69 sample group was sent to Galbraith Laboratories, Inc. in Knoxville, TN. The instrument utilized was a PerkinElmer Avio 500 for the ICP-OES vaporization process, with the Optima 3300DV, Optima 4300DV, 5300, and 8300 for emission

wavelength measurement. The power was set to 1500 Watts, and the plasma view was radial. To synthesize the sample solution, the sample was fused with sodium peroxide over Bunsen burner, then followed by a dissolution in water. Then the solution was acidified using both nitric acid and hydrochloric acid. The final volume of the solutions was 100mL each.

The speed of the aerosols entering the ICP-OES instrument were 10 L/min for the plasma gas, 0.2 L/min for the auxiliary gas, and 0.7 L/min for the nebulizer gas.

4.5 ATTENUATED TOTAL REFLECTANCE COUPLED WITH FOURIER TRANSFORM INFRARED (ATR-FTIR)

A Cary 60 Model ATR-IR spectrometer was used to record the ATR-IR spectra of the CAT-69 sample group along with a bentonite control. For each specimen 128 scans were performed at a resolution of 8 cm^{-1} in the range of $4000\text{-}650\text{ cm}^{-1}$.

4.6 VISCOSITY

The viscosity test was performed using a ViscoQC 100R from Anton Paar. All of the measurement types were single point with a DG 26 spindle at a speed of 5 rpm with a sample volume of 7.5 mL. Three samples were measured, with a bentonite clay slurry control, a bentonite-Betaine clay slurry, and a bentonite-Betaine-Ag clay slurry, with the detailed composition shown in Table 2.

Table 2: The compositions of the samples that were utilized in viscosity testing.

Sample	Clay (mole)	DI water (moles)	Betaine (mole)	AgNO₃ (mole)
Bentonite Slurry	7.81×10^{-3}	2.78	0	0
Bentonite-Betaine slurry	7.81×10^{-3}	2.78	4.93×10^{-3}	0

Bentonite-Betaine-Ag slurry	7.81×10^{-3}	2.78	4.93×10^{-3}	1.77×10^{-3}
------------------------------------	-----------------------	------	-----------------------	-----------------------

The synthesis of these slurries followed the standard clay film formation procedure sans pouring and drying to analyze the viscosity of the clay slurries. The torque required for the spindle to turn against the slurry as a percentage was reported and used to calculate the viscosities of the slurries.

4.2 BACTERIOCIDAL EFFICACY

Following peeling of the clay film, the antibacterial efficacy was tested against both gram-positive bacteria and gram-negative bacteria of the control clay film and the silver clay film using the Kirby-Bauer disc diffusion test. The CAT-69 sample group was used to test the antibacterial efficacy as compared to the control sample AB-1-13. The films were punched into 0.5 cm diameter disks that were sterilized with UV radiation. *Staphylococcus aureus* and *Escherichia coli* were inoculated in Luria-Bertani (LB) broth and shaken at 120 rpm at 37 °C until an optical density of 600 nm was measured using a UV-vis spectrophotometer. Then, the optical density was adjusted to 0.1 nm before 30 µL was plated on an LB agar plate as a lawn along with the sample disks. The zones of inhibition were studied using the Kirby-Bauer disc susceptibility test.

CHAPTER 5: RESULTS

5.1 CLAY FILM FORMATION

The Betaine concentration greatly alters the final qualitative properties of the clay film. Specifically, the Betaine affects the texture of the final clay product, with greater concentrations of Betaine corresponding to films that more easily adhere to themselves.

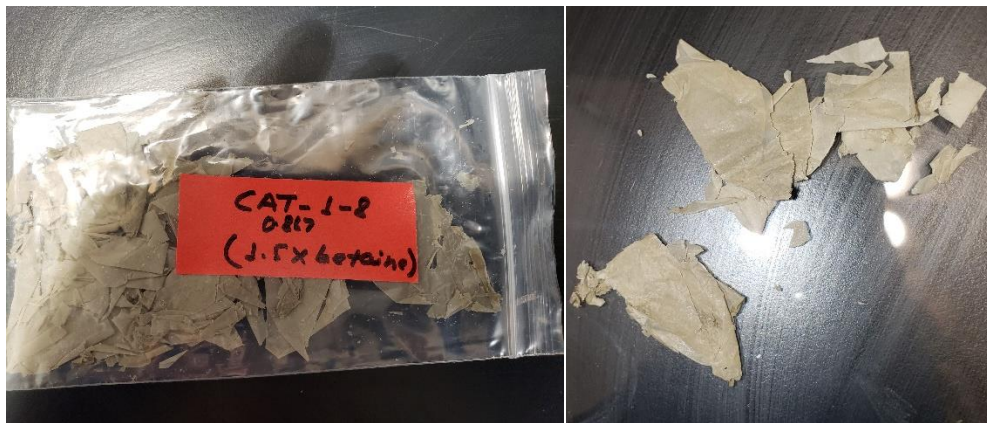


Figure 4: Sample CAT-8 after peeling in bag (left) and on glass plate (right)

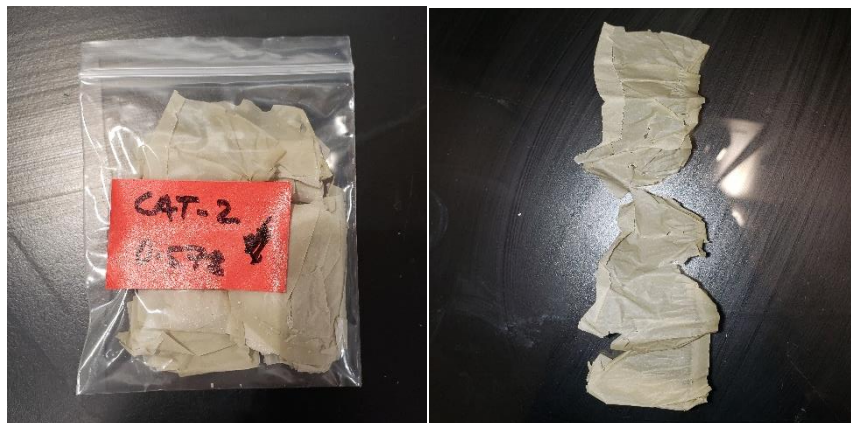


Figure 5: Sample CAT-2 after peeling in bag (left) and on glass plate (right)



Figure 6: Sample CAT-7 after peeling in bag (left) and on glass plate (right)

A concentration of Betaine that is too low will cause the clay films formed to be fragile, or not form clay films at all, instead splintering when attempting to peel the films off the glass plate, which can be seen in Figure 4, with sample CAT-8. A concentration of Betaine that is too high, on the other hand, will cause the clay films that form to be difficult to handle due to the stickiness of the final product, which can be seen in Figure 5, with sample CAT-2. Following the synthesis of clay films with differing amounts of Betaine, the most effective sample was found to contain 2.47×10^{-3} moles of Betaine, which corresponds to Figure 6, with sample CAT-7. This Betaine concentration formed a clay film that was stable enough to be handled as well as did not aggregate to the point of being unusable. Most samples made after CAT-7 used 2.47×10^{-3} moles of Betaine, with some samples being altered for testing with additions of silver. However, it was found that the 2.47×10^{-3} moles still consistently formed the most stable clay films. Accordingly, the majority of clay films followed this concentration of Betaine with some modulations. With the optimal synthesis of clay films developed, the following analytical methods were utilized to determine the success of incorporation of both the Betaine zwitterions and silver cations. The sample group used

for the majority of the testing included the CAT-69 group, CAT-69 (Ag-1), CAT-69 (Ag-2), CAT-69 (Ag-3), and CAT-69 (Ag-4). These samples used the standard 2.47×10^{-3} moles of Betaine, but each included a different concentration of silver ions, with CAT-69 (Ag-1) containing the lowest initial silver nitrate, 8.83×10^{-4} moles, and the values increasing to 2.65×10^{-3} moles for CAT-69 (Ag-2), 5.30×10^{-3} moles for CAT-69 (Ag-3), and 1.06×10^{-2} moles for CAT-69 (Ag-4)

5.2 X-RAY PHOTOELECTRON SPECTROSCOPY (XPS)

The XPS analyses were utilized with clay film samples containing differing amounts of Betaine and silver to initially detect the presence of nitrogen from Betaine and silver cations. While other, more accurate methods were later utilized to determine the concentrations of each element or compound. Specific binding energies detected can be used to confirm the presence of Betaine and silver. Nitrogen can be detected with its 1s orbital, which can be used to determine the presence of Betaine, and the 3d orbital of silver can be detected. Table 3 shows the significant binding energies expected in this experiment along with the interpretation of those binding energies.

Table 3: XPS binding energy values and their corresponding element and interpretation that are of interest to this experiment

XPS Value	Corresponding Element	Interpretation
401.6 eV ³⁷	Alkyl Ammonium (NR ₄ ⁺) N 1s	The organo-functionalization of the clay with Betaine was successful
373.8 eV ³⁷	Ag 3d _{5/2} ³⁷	The incorporation of silver into the clay through cation exchange was successful
368.2 eV ³⁷	Ag 3d _{3/2} ³⁷	The incorporation of silver into the clay through cation exchange was successful

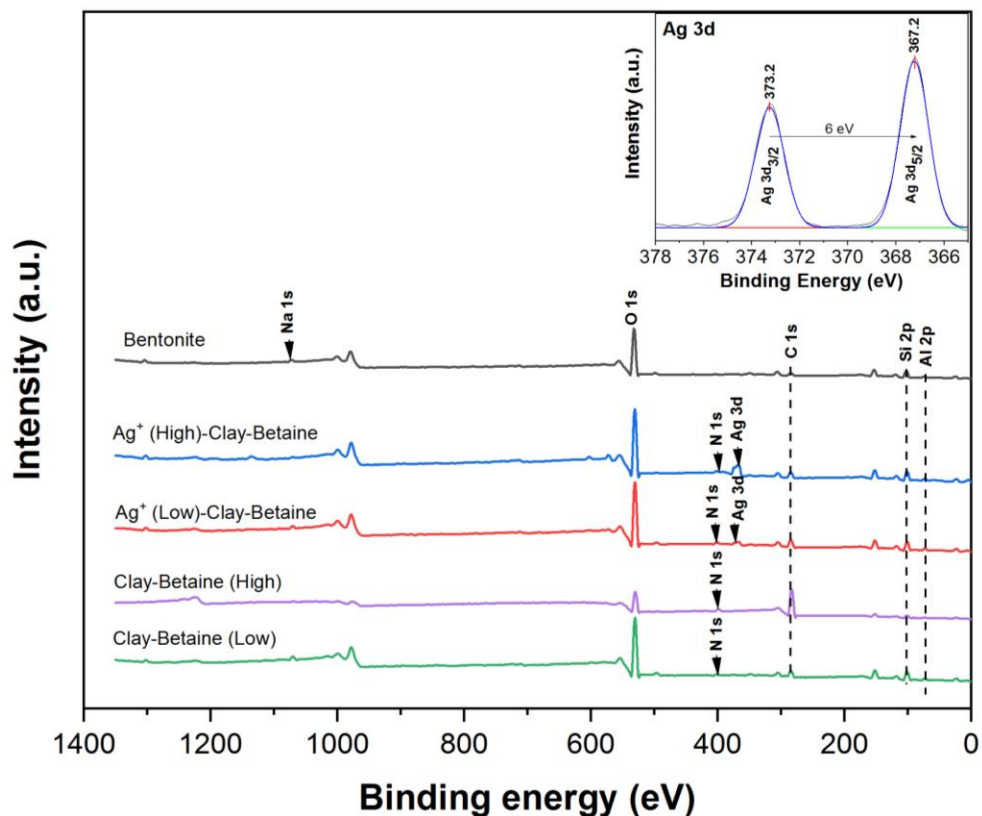


Figure 7: XPS survey scan for Bentonite (control), Ag⁺ (High conc.)-Clay-Betaine, Ag⁺ (Low conc.)-Clay-Betaine, Clay-Betaine (High conc.), and Clay-Betaine (Low conc.).

It can be observed in the XPS graphical data in Figure 7 that there were significant peaks for nitrogen at 400 eV and for silver ions at 373.2 eV and 367.2 eV. These values indicate that the Betaine and silver were successfully incorporated into the clay matrix.³⁷

5.2 POWDER X-RAY DIFFRACTION (XRD)

The XRD data demonstrates the alteration of the d_{001} -spacing by Betaine. This indicates that the use of the zwitterion had a significant effect on the structure of the synthesized clay film that caused an expansion. Equation [2] was used to calculate the d_{001} -spacing, with the outcome charted in Table 4. There was no significant d_{001} peak seen for the bentonite control. This lack of

d peak in the control and the presence of Betaine, as confirmed by other analysis including XPS and ATR-FTIR, indicate that the expanded spacing between the clay layers due to the presence of Betaine. Overall, it can be realistically inferred that the expanded d -spacing due to Betaine results in the formation of usable clay films. Figure 8 is the graphical representation of the XRD data with the d_{001} values denoted for each sample. Table 4 shows the values from the XRD analysis utilized to calculate the d_{001} -Value along with the d_{001} -Value for each sample. The previously stated CAT-69 sample group was utilized in this XRD analysis.

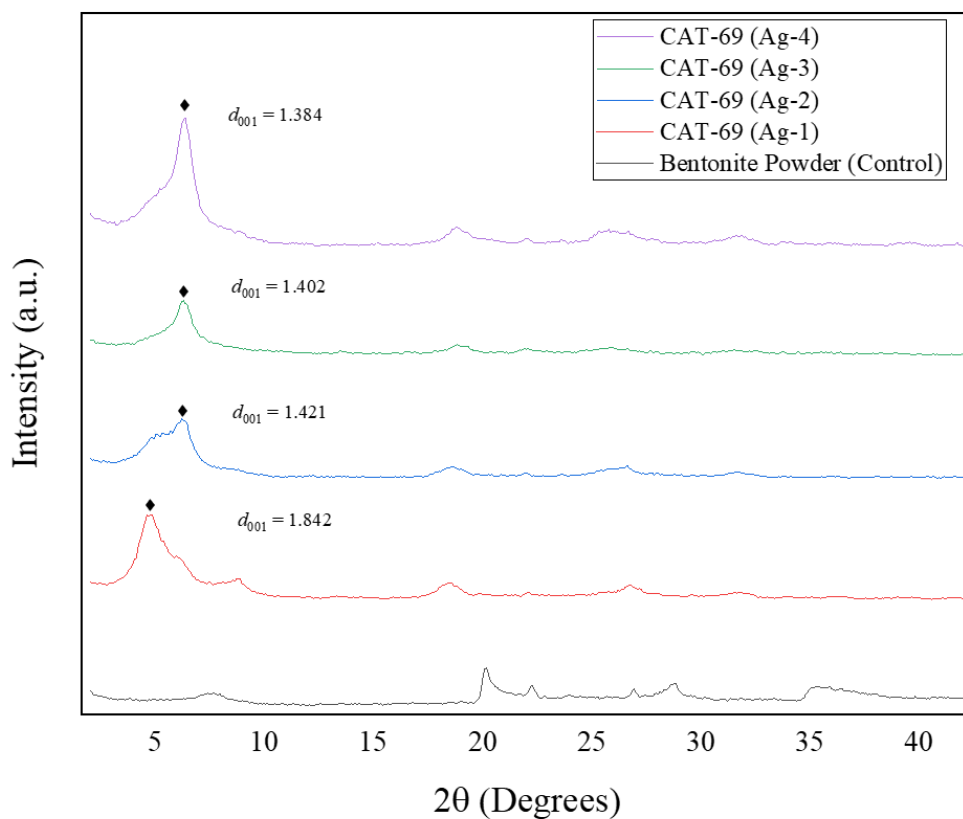


Figure 8: XRD data for CAT-69 (Ag-1), CAT-69 (Ag-2), CAT-69 (Ag-3), CAT-69 (Ag-4), and the Bentonite Control

Table 4: d_{001} -Values for the XRD data and the corresponding values that were used in calculations for the d_{001} -Values.

Sample	λ	2θ (d_{001})	θ (d_{001})	d_{001} -value as calculated from equation [2] (nm)
Bentonite clay (control)	0.1540598	Amorphous	-	-
CAT-69 (Ag-1)	0.1540598	4.792337	2.396	1.842
CAT-69 (Ag-2)	0.1540598	6.2127947	3.103	1.421
CAT-69 (Ag-3)	0.1540598	6.29635103	3.148	1.402
CAT-69 (Ag-4)	0.1540598	6.379907	3.190	1.384

The d_{001} peak for each sample and the resulting calculations shows that the interlayer spacing between the clay layers was successfully expanded presumably due to the incorporation of Betaine within the clay matrix when compared to the bentonite powder control, and the incorporation of silver does not significantly disrupt the resulting expansion.

5.3 X-RAY FLUORESCENCE SPECTRA (XRF)

The XRF data shows that the final silver content in the films increased as the initial silver incorporated increased, and there did not appear to be an upper limit with the different silver concentrations utilized in this endeavor. While the XRF data is helpful as a preliminary step, it is qualitative and can be inaccurate, and was followed by an ICP-OES analysis. The XRF data can be seen in Table 5.

Table 5: Chemical composition of Ag-clay sample (in percentage)

Sample	Al	Si	Ca	Fe	Ag
CAT-69 (Ag-1)	21.631%	72.850%	1.659%	3.629%	0.232%

CAT-69 (Ag-2)	21.883%	73.101%	1.370%	3.305%	0.340%
CAT-69 (Ag-3)	20.603%	74.764%	0.850%	3.257%	0.525%
CAT-69 (Ag-4)	15.806%	64.755%	9.165%	8.175%	2.099%

5.4 INDUCTIVELY COUPLED PLASMA-OPTICAL EMISSION SPECTROSCOPY (ICP-OES)

With the ICP-OES data, it is evident that the silver content of the final hybrid films increases with increasing initial silver concentrations. With the quantitative data from ICP-OES, the silver concentration can be clearly analyzed. The ICP-OES data is illustrated in Table 4.

Table 6: ICP-OES data

Sample	Silver Percentage	Sample Amount Used	Amount of Silver in Sample	Sample Concentration	Silver Concentration
CAT-69 (Ag-1)	2.78%	29.75 mg	0.827 mg	29.75 g/L	7.67 mM
CAT-69 (Ag-2)	4.78%	25.79 mg	1.424 mg	25.79 g/L	13.20 mM
CAT-69 (Ag-3)	7.96%	26.79 mg	2.132 mg	26.79 g/L	19.76 mM
CAT-69 (Ag-4)	6.49%	25.53 mg	1.657 mg	25.53 g/L	15.36 mM

5.5 FOURIER-TRANSFORM INFRARED SPECTROSCOPY (ATR-FTIR)

The ATR-FTIR data can be viewed in Figure 9. While some samples were not included in the figure for graphical clarity, CAT-69 (Ag-2) and CAT-69 (Ag-3) generally follow the trends of CAT-69 (Ag-1) and CAT-69 (Ag-4). Specifically, peaks in the 1600 cm^{-1} region are characteristic

of carboxyl bond antisymmetric stretching, peaks in the 1400 cm^{-1} region are characteristic of C-N bond stretching, and peaks in the 1330 cm^{-1} region are characteristic of N-C-H bond stretching.

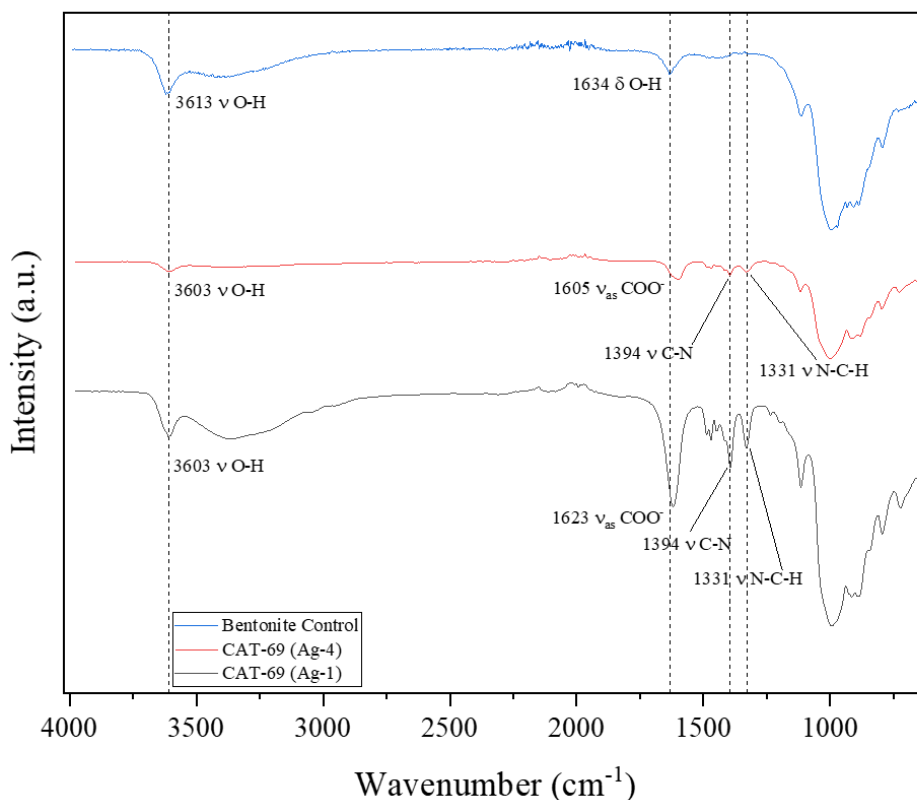


Figure 9: ATR-IR of sample CAT-69 (Ag-1), CAT-69 (Ag-4), and the bentonite control.

5.6 VISCOSITY

To analyze the viscosity of the samples, the torque needed to stir against the slurry was found for each sample, with the viscosity being directly related to the torque. The samples tested were the bentonite slurry, which was composed of 7.81×10^{-3} moles of clay in water, the bentonite-Betaine slurry, which was composed of 7.81×10^{-3} moles of clay in addition to 4.93×10^{-3} moles of Betaine, and finally, the bentonite-Betaine-ag slurry, which was composed of 7.81×10^{-3} moles

of clay, $.93 \times 10^{-3}$ moles of Betaine, and 1.77×10^{-3} moles of silver. The viscosity results of these samples should provide a good representation for the interactions between clay, bentonite, and silver in solution. The viscosity results are shown in Table 7, with both the torque and resulting viscosity reported.

Table 7: Viscosity data

Sample	Torque	Viscosity
Bentonite Slurry	69.7 %	105 cP
Bentonite-Betaine Slurry	8.0 %	84 cP
Bentonite-Betaine-Ag Slurry	72.6 %	58.08 cP

5.7 KIRBY-BAUER

The results of the Kirby-Bauer disc diffusion are shown in Figures 10, 11, 12, and tables 8 and 9. From these results, it is shown that the clay matrices with silver had significant antibacterial effects on both the gram-positive (*S. aureus*) and gram-negative (*E. coli*) tests. The control samples

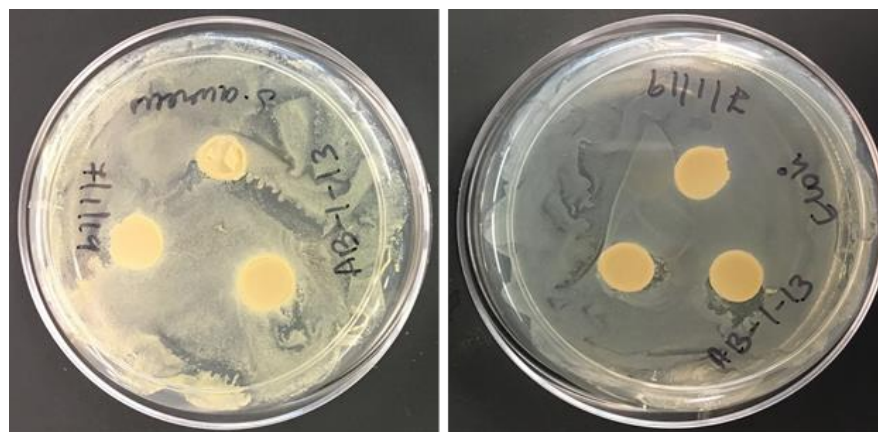


Figure 10: Control Samples AB-1-13 Kirby-Bauer disc diffusion against *S. aureus* (Left) and *E. coli* (Right).

only contained the clay-Betaine complex without any silver cation integration. The disc size used in the experimentation were 0.6 cm in diameter.

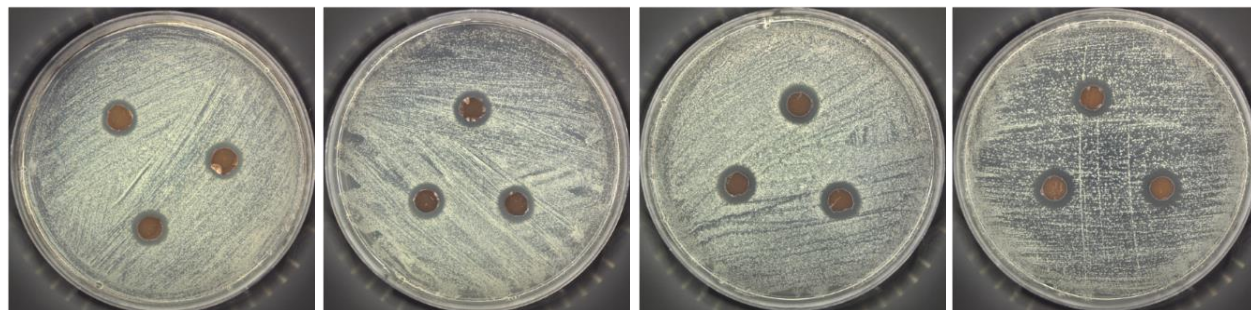


Figure 11: From left to right, samples CAT-69 (Ag-1), CAT-69 (Ag-2), CAT-69 (Ag-3), and CAT-69 (Ag-4) Kirby-Bauer disc diffusion against *S. aureus*.

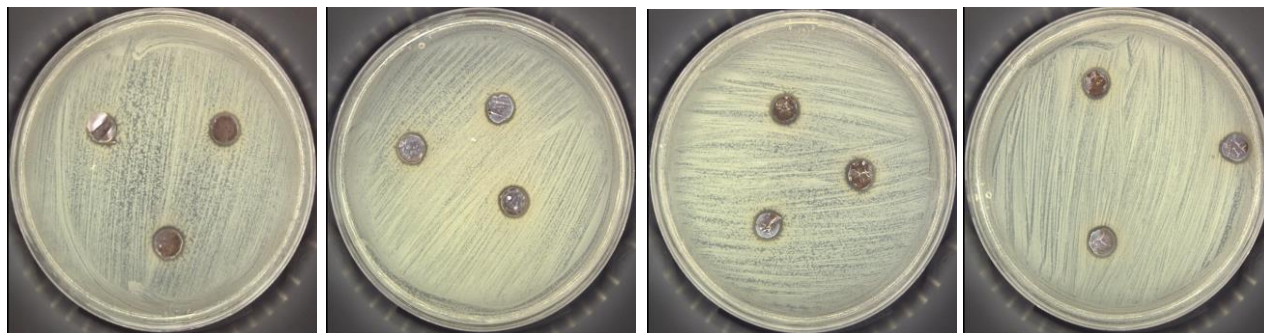


Figure 12: From left to right, samples CAT-69 (Ag-1), CAT-69 (Ag-2), CAT-69 (Ag-3), and CAT-69 (Ag-4) Kirby-Bauer disc diffusion against *E. coli*.

Table 8: Data for the Kirby-Bauer disc diffusion against *S. aureus*.

Sample Name	Zone 1 (cm)	Zone 2 (cm)	Zone 3 (cm)	Average	S.D.
AB-1-13	0	0	0	0	0
CAT-69 (Ag-1)	1.2	1.2	1.2	1.2	0
CAT-69 (Ag-2)	1.2	1.2	1.2	1.2	0
CAT-69 (Ag-3)	1.3	1.3	1.3	1.3	0
CAT-69 (Ag-4)	1.3	1.3	1.3	1.3	0

Table 9: Data for the Kirby-Bauer disc diffusion against *E. coli*.

Sample Name	Zone 1 (cm)	Zone 2 (cm)	Zone 3 (cm)	Average	S.D.
AB-1-13	0	0	0	0	0
CAT-69 (Ag-1)	1	1	1	1	0
CAT-69 (Ag-2)	1	1	1	1	0
CAT-69 (Ag-3)	1	1	1	1	0
CAT-69 (Ag-4)	1	1	1	1	0

The clay control samples that did not contain silver ions lacked a zone of inhibition, which indicates that the clay films with only Betaine do not have antibacterial properties. Contrary, the clay samples containing silver ions had significant zones of inhibition, with a 1 cm zone of inhibition for the *E. coli* samples, and at least a 1.2 cm zone of inhibition for the *S. aureus* samples. This outcome demonstrates that the hybrid clay films indeed possess antimicrobial activity, and that antimicrobial activity can be attributed to the presence of silver in the functionalized clay samples.

CHAPTER 6: DISCUSSION

6.1 CLAY FILM FORMATION

After the experimental modulation of the composition of the clay films, the ideal amount of Betaine that needed to be added to the clay film was determined to be 2.47×10^{-3} moles of Betaine. In addition, the amount of silver (Ag) ions added did not seem to significantly alter the final clay film structure, with it depending primarily upon the initial Betaine concentration.

The final clay films formed in this effort were the result of incorporating a calculated amount of betaine that produced films that had optimal tackiness and robustness.

6.2 X-RAY FLUORESCENCE (XRF)

According to the XRF data, the silver content in the clay films increased as the initial silver ion concentration was increased, which indicates the successful cation exchange of silver ions with sodium ions in the clay layers. However, as previously stated, the XRF data is valuable as a preliminary, qualitative analysis followed by ICP-OES to further confirm the successful cation exchange.

6.3 INDUCTIVELY COUPLED PLASMA-OPTICAL EMISSIONS SPECTROSCOPY (ICP-OES)

The ICP-OES analysis provided a more accurate, quantitative measurement of the composition of the final clay films. In the ICP-OES data, there is obvious inclusion of silver in the final composition. In addition, the silver was detected at significant percentages. It appears that at lower concentrations, the amount of silver nitrate added initially is directly related to the final

concentration of silver detectable in the final products. In the analyzation of CAT-69 (Ag-1), CAT-69 (Ag-2), and CAT-69 (Ag-3), this trend is obvious.

Table 10: ICP-OES Silver Data

Sample	Initial AgNO ₃ (moles)	Expected Concentration Ag (%)	Actual Concentration from ICP-OES (Ag %)
CAT-69 (Ag-1)	8.83×10^{-4}	1X	2.78%
CAT-69 (Ag-2)	2.65×10^{-3}	3X	4.78%
CAT-69 (Ag-3)	5.30×10^{-3}	6X	7.96%
CAT-69 (Ag-4)	1.06×10^{-2}	12X	6.49%

Evidently, the silver percentages within the clay matrix increased with increasing initial silver concentrations. This increase of silver concentrations corresponds to an increase in interlayer spacing in the clay allowing for cation exchange with silver, which can be characterized through XRD.

6.4 X-RAY DIFFRACTION (XRD)

The powder XRD data showed that the engineered clay films had significant structural changes when compared to the bentonite powder control. Specifically, the d_{001} -spacing was measured to be present and more stable within the clay samples with Betaine and silver. This indicates that the spacing within the clay layers was significantly increased through the addition of Betaine, which matches the theoretical role of a zwitterion within clay layers.⁸

The silver cation is relatively large when compared to the sodium ion. Therefore, a greater basal spacing is required for the exchange of silver ions for sodium ions, which can be achieved by the expansion of the d_{001} -spacing by Betaine. Overall, the powder XRD data shows that Betaine can increase the space between clay layers, and the spaces between those layers are not disrupted

by the cationic exchange of silver.³⁸ This analyzation demonstrates the underlying physical structure of the stable clay films synthesized in this thesis.

6.5 X-RAY PHOTOELECTRON SPECTROSCOPY (XPS)

The XPS gave an initial indication of the presence of silver (II) species and nitrogen. A peak at 400 eV is associated with nitrogen in its 1s orbital, which can be seen in the analyzed samples.³⁷ The only source of nitrogen in this experiment was from the Betaine molecules. Resultingly, the presence of nitrogen indicates the presence of Betaine. Another objective of the XPS was to identify the presence of silver (I) ions through the binding energy peaks at 372.6 eV and 366.9 eV, which match the binding energy of silver cations in the *d* orbital.³⁷

6.6 VISCOSITY

The viscosity analyses provided important information about the interaction between the clay layers, Betaine zwitterion, and the silver in slurry or solution. The decrease in viscosity when Betaine was introduced implies the disruption of clay floc van der Waals interactions within the slurry by the Betaine, and the further decrease in viscosity when silver nitrate was added shows interaction between the silver ions, the clay, and the Betaine.⁸ Overall, this shows there is significant interaction between the clay, the Betaine, and the silver, enough to disrupt clay flocs within solution.

6.7 BIOLOGICAL TESTING

The Kirby-Bauer disc diffusion test for *S. aureus* shows a significant zone of inhibition for every CAT-69 sample, with a greater zone of inhibition for CAT-69 (Ag-3) and CAT-69 (Ag-4).

Comparing the Kirby-Bauer results with the ICP-OES analysis, it appears that increasing silver concentration does affect the antibacterial efficacy of the clay films; however, it seems that significant differences in silver concentrations are needed to cause differences in film antibacterial properties. The analysis demonstrated that the samples with the upper values of silver had a similar percentage, which corresponds with the bacterial testing showing that the two samples had comparable efficacy when testing with *S. aureus*. The Kirby-Bauer disc diffusion test for *E. coli* also demonstrated the antibacterial efficacy of the clay-silver hybrid films against the gram-negative bacterial sample. In addition, the zone of inhibition for all the samples against *E. coli* were the same. This demonstrates that increasing the silver concentration is not necessarily required to increase the antibacterial efficacy of the silver films. Consequently, the amount of silver used can be moderated, combatting both expenses and antibacterial resistance to silver cations, creating an effective and cheap solution to healing wounds.

CHAPTER 7: CONCLUSION

Overall, this research serves as an entry to the possible usage of organo-functionalized clay films as a bandage system. A highly cost-effective bandage system can be synthesized using clay, antibacterial silver, and Betaine. Compared to the current FDA-approved treatments, this bandage system has the potential to utilize less silver overall, which can help combat both antibacterial resistances forming as well as cytotoxicity due to introductions of high amounts of silver to the body.

Through the use of XRF, ICP-OES, XRD, XPS, viscosity measurements, and antimicrobial testing, it can be determined that a stable clay film with antibacterial properties can be synthesized with the goal to provide antibacterial resistance in a stable bandage form. The analytical methods showed that Betaine was successfully incorporated, as demonstrated in the ATR-FTIR with the values near 1400 cm^{-1} and 1330 cm^{-1} , and the XPS with values near 400 eV, which indicate the presence of carbon-nitrogen bonds, and nitrogen alone, respectively, which only be provided from the presence of Betaine. In addition, the XRD showed that Betaine created sufficient d_{001} -spacing within the clay matrix. The presence of silver was confirmed by the XPS peak at about 400 eV and the ICP-OES analysis. Finally, the viscosity analysis confirmed that both Betaine and silver induce structural changes in solution in the clay layers, demonstrating that there is structural interaction between the clay layers, Betaine, and silver ions.

The antibacterial assays revealed zones of inhibitions indicating that the films with incorporated silver inhibited the growth of the gram-positive bacteria, whereas the clay film control lacking silver had no zone of inhibition. Therefore, the results of this experimentation

demonstrate that clay films can act as a stable vehicle for silver, which acts as an antibacterial agent. This combination creates an affordable alternative to current silver treatments by using a cheap vehicle for antibacterial release as well as limiting the amount of silver present to only the amount needed to act as an antibiotic, which will also combat antibiotic resistance.

Therefore, this research has definitively developed an antibacterial silver-clay hybrid film by taking advantage of the natural characteristics of clay, the molecular attributes of Betaine, and the antibacterial efficacy of silver cations. This outcome indicates the possibility of synthesizing a cheap, clay-based antibacterial bandage system to treat wounds.

CHAPTER 8: MOVING FORWARD

Following this research, several steps can be taken to further investigate the antimicrobial efficacy of the synthesized hybrid clay films, such as live animal studies. By proving that hybrid silver-clay films have significant antibacterial activity *in vitro*, the next step is to investigate the *in vivo* properties of these clay matrices. The formulation of the bandages utilizing these clay films will also be developed, with a hypothetical bandage system utilizing adhesive edges around a clay film center.

In addition, there are studies being done to investigate the catalytic abilities of clay matrices and the ability of these clay matrices to act as a battery source. These different experimental studies are being investigated to determine the ability for clay matrices to be used in different ways within the body.

These future works will further advance the fundamentals studied in this work and apply them to new techniques and technologies that have the potential to provide newer, cheaper ways to treat a variety of wounds.

REFERENCES

1. World Health Organization. Burns. <https://www.who.int/news-room/fact-sheets/detail/burns>
2. Jeschke, M.G.; van Baar, M.E.; Choudhry, M.A.; Chung, K.K.; Gibran, N.S.; Logsetty, S. Burn Injury. *Nature Reviews: Disease Primers*, **2020**, *6*, 1-25.
3. Liu, H.F.; Zhang, F.; Lineaweaver, W. C. History and Advancement of Burn Treatment. *Annals of Plastic Surgery* **2017**, *78*, S2-S8.
4. Dário, G.M.; Silva, G.G.; Gonçalves, D.L.; Silveira, P; Teixeira, A.; Angioletto, E.; Bernardin, A.M. Evaluation of the healing activity of therapeutic clay in rat skin wounds.
5. Sahin, I.; Ozturk, S.; Alhan, D.; Açikel, C.; Isik, S. Cost Analysis of Acute Burn Patients Treated in a Burn Center: The Gulhane Experience. *Annals of Burns and Fire Disaster* **2011**, *24*, 9-13.
6. Chiu, F.-C.; Lai, S.-M.; Hsieh, I.-C.; Don, T.-M.; Huang, C.-Y. Preparation and Properties of Chitosan/Clay (Nano)Composites: A Silanol Quaternary Ammonium Intercalated Clay. *Journal of Polymer Research* **2012**, *19*, 1-11.
7. Gan C, Hu H, Meng Z, et al. Characterization and Hemostatic Potential of Two Kaolins from Southern China. *Molecules* **2019**, *24*.
8. Schmidt, C. U.; Lagaly, G. Surface Modification of Bentonites: I. Betaine Montmorillonites and their Rheological and Colloidal Properties. *Clay Minerals* **1998**, *34*, 447-458.
9. National Institute of General Medical Sciences. Burns. *USA Department of Health and Human Services* **2018**. <https://www.nigms.nih.gov/education/fact-sheets/Pages/burns.aspx>
10. U.S. National Library of Medicine. Medline Plus. Skin Graft. <https://medlineplus.gov/ency/article/002982.htm>. (accessed Oct. 24, 2020)

-
11. Tiwari, V.K. Burn Wound: How it differs from other wounds? *Indian Journal of Plastic Surgery*, **2012**, *45*, 364-373.
 12. Dwivedi, S.; Tiwari, P. Burn Wound: An update focusing the classification, Immune responses and management resources aid in healing. *Research Journal of Science and Technology*, **2014**, *6*, 128-132.
 13. Xiu, F.; Jeschke, M.G. Perturbed mononuclear phagocyte system in severely burned and septic patients. *Shock* **2013**, *40*, 81-88.
 14. Huan, Z.; Zhuang, D.; Xiong, B.; Deng, D.X.; Li, H.; Lai, W. Occupational exposure to SARS-CoV-2 in burns treatment during the COVID-19 epidemic: Specific diagnosis and treatment protocol. *Biomedicine & Pharmacotherapy* **2020**, *127*.
 15. Schoonheydt, R.A.; Johnson, C.T.; Bergaya, F. Clay Minerals and their Surfaces. *Developments in Clay Sciences* **2018**, *9*, 1-21.
 16. Jeon, I.; Nam, K. Change in the Site Density and Surface Acidity of Clay Minerals by Acid or Alkali Spills and its Effect on pH Buffering Capacity. *Scientific Reports*. **2019**. *9*.
 17. Ray, S.S.; Okamoto, M. Polymer/Layered Silicate Nanocomposites: A Review from Preparation to Processing. *Progress in Polymer Science* **2003**. *28*, 1539-1641.
 18. Majka, T.M.; Pielichowski, K. Functionalized Clay-Containing Composites. In *Polymer Composites with Functionalized Nanoparticles*; Elsevier, 2019; 149-278.
 19. Schulze, D.G. Clay Minerals. In *Encyclopedia of Soils in the Environment*; Hillel, D.; Elsevier, 2005; 246-254

-
20. Li, Y.; Wei, S.; Xu, N.; H, Y. Internal Forces within the Layered Structure of Na-Montmorillonite Hydrates: Molecular Dynamics Simulation. *The Journal of Physical Chemistry*. **2020**, *124*, 25557-25567.
 21. Zhu, T. T.; Zhou, C. H.; Kabwe, F. B., Wu, Q. Q.; Li, C. S.; Zhang, J. R. Exfoliation of Montmorillonite and Related Properties of Clay/Polymer Nanocomposites. *Applied Clay Science*. **2019**. *169*, 48-66.
 22. Chapman, H.D. Cation-Exchange Capacity. In *Methods of Soil Analysis: Part 2 Chemical and Microbiological Properties*; Norman, A.G., Eds.; American Society of Agronomy: Madison, Wisconsin. 1965; 149-278.
 23. Majka, T.M.; Pielichowski, K. Functionalized Clay-Containing Composites. In *Polymer Composites with Functionalized Nanoparticles*; Elsevier, 2019; 149-278.
 24. National Library of Medicine. Betaine. *PubChem*.
 25. Otto, C.C.; Haydel, S.E. Exchangeable Ions Are Responsible for the *In Vitro* Antibacterial Properties of Natural Clay Mixtures. *PLOS One* **2013**, *8*, 1-9.
 26. Williams, L.B.; Metge, D.W.; Eberl, D.D; Harvey, R.W.; Turner, A.G.; Prapaipong, P.; Poret-Peterson, A.T. What Makes a Natural Clay Antibacterial? *Environmental Science & Technology* **2011**, *45*, 3766-3773.
 27. Chiu, F.-C.; Lai, S.-M.; Hsieh, I.-C.; Don, T.-M.; Huang, C.-Y. Preparation and Properties of Chitosan/Clay (Nano)Composites: A Silanol Quaternary Ammonium Intercalated Clay. *Journal of Polymer Research* **2012**, *19*, 1-11.

-
28. Yilmaz Atay H. Antibacterial Activity of Chitosan-Based Systems. *Functional Chitosan* **2020**, 457-489.
29. Nigmatullin, R.; Gao, F.; Konovalova, V. Polymer-Layered Silicate Nanocomposites in the Design of Antimicrobial Materials. *Journal of Materials Science* **2008**, *43*, 5728-5733.
30. Park, J.-H.; Shin, H.-J.; Kim, M. H.; Kim, J.-S.; Kang N.; Lee, J.-Y.; Kim, K.-T.; Lee, J. I.; K, D. Application of Montmorillonite in Bentonite as a Pharmaceutical Excipient in Drug Delivery Systems. *Journal of Pharmaceutical Investigation* **2016**, *46*, 363-375.
31. Maillard, J.; Hatermann, P. Silver as an antimicrobial: Facts and gaps in Knowledge. *Critical Reviews in Microbiology* **2013**, *39*, 373-383.
32. Frei, A.; Zuegg, J.; Elliot, A.G.; Baker, M.; Braese, S.; Brown, C.; Chen, F.; Dowson, C.G.; Dujardin, G.; Jung, N.; King, A.P.; Mansour, A.M.; Massi, M.; Moat, J.; Mohamed, H.A.; Renfrew, P.J.; Sadler, P.J.; Todd, M.H.; Willans, C.E.; Wilson, J.J.; Cooper, M.A.; Blaskovich, M.A.T. Metal Complexes as a promising source for new antibiotics. *Chemical Science* **2020**, *12*, 2627-2639.
33. Yasuyuki, M.; Kunihiro, K. Kurissery, S.; Kanavillil, N.; Sato, Y.; Kikuchi, Y. Antibacterial Properties of Nine Pure Metals: A Laboratory Study using *Staphylococcus aureus* and *Escherichia coli*. *Biofouling*, **2010**, *26*, 851-858.
34. Monteiro, D.R.; Gorup, L.F.; Takamiya, A.S.; Ruvollo-Filho, A.C.; de Camargo, E.R.; Barbosa, D.B. The growing importance of materials that prevent microbial adhesion: antimicrobial effect of medical devices containing silver. *International Journal of Antimicrobial Agents* **2009**, *34*, 103-110

-
35. Umemura, Y. Preparation and application of clay mineral films. *Developments in Clay Science* **2018**, *9*, 377-396.
 36. Greczynski, G.; Hultman, L. X-Ray Photoelectron Spectroscopy: Towards Reliable Binding Energy Referencing. *Progress in Materials Science*, **2020**, *107*, 100591.
 37. NIST X-Ray Photoelectron Spectroscopy Database, Version 4.1 (National Institute of Standards and Technology, Gaithersburg, **2012**; <http://srdata.nist.gov/xps/>).
 38. Stanjek, H.; Häusler, W. Basics of X-Ray Diffraction. *Hyperfine Interactions*, **2004**, *154*, 107-119.
 39. Schlotz, R.; Uhlig, S. Introduction to X-Ray Fluorescence (XRF). *Bruker Advanced X-Ray Solutions*, **2000**.
 40. Thomsen, V. Basic Fundamental Parameters in X-Ray Fluorescence. *Spectroscopy* **2007**. *22*, 46-50.
 41. Holmes, G.S. The Limitations of Accurate “Thin-Film” X-Ray Fluorescence Analysis of Natural Particular Matter: Problems and Solutions. *Chemical Geology*, **1981**. *33*, 333-353.
 42. Olesik, J.W. Fundamental Research in ICP-OES and ICPMS. *Analytical Chemistry News and Features*, **1996**. *68*, 469A-474A.
 43. Hashimoto, K.; Badarla, V.R.; Ideguchi, T. High-Speed Fourier-Transform Infrared Spectroscopy with Phase-Controlled Delay Line. *Laster & Photonics Reviews*, **2021**, *15*, 2000374.
 44. Hind, A.R.; Bhargava, S.K.; McKinnon, A. At the solid/liquid interface: FTIR/ATR – the tool of choice. *Advances in Colloid and Interface Science* **2001**, *93*, 91-114.

-
45. Schuttlefield, J. D.; Grassian, V. H. ATR-FTIR Spectroscopy in the Undergraduate Chemistry Laboratory. *Journal of Chemical Education*. **2008**, *85*, 279-281.
46. Swartzen-Allen, S.L.; Matijević, E. Surface and Colloid Chemistry of Clays. *Chemical Reviews*. **1974**, *74*, 385-400
47. Shapovalov, V. Characterization of Polymer/Clay Nanocomposites. Ph. D. Dissertation, The City University of New York, **2003**.
48. Sizar, O.; Unakal, C.G. Gram-positive Bacteria. *Stat Pearls* **2020**.
49. Hudzicki, J.; Kirby-Bauer Disk Diffusion Susceptibility Test Protocol. *American Society for Microbiology* **2009**